

Lepton flavor violating Z decays: A promising window to low scale seesaw neutrinos

V. De Romeri,^{*} M. J. Herrero,[†] X. Marcano,[‡] and F. Scarcella[§]

*Departamento de Física Teórica and Instituto de Física Teórica, IFT-UAM/CSIC,
Universidad Autónoma de Madrid, Cantoblanco, 28049 Madrid, Spain*

(Received 2 December 2016; published 21 April 2017)

In this paper we study the lepton flavor violating Z boson decays $Z \rightarrow \tau\mu$ and $Z \rightarrow \tau e$ in the context of low scale seesaw models with new heavy Majorana neutrinos whose masses could be reachable at the LHC. Our computations of the decay rates are done in the particular realization given by the inverse seesaw model with six extra heavy neutrinos which are quasidegenerate in three pseudo-Dirac pairs. In particular, we focus on scenarios that are built *ad hoc* to produce suppressed rates in all the processes involving μ - e transitions, given the fact that these are by far the most strongly constrained by present data. We will fully explore the $Z \rightarrow \tau\mu$ and $Z \rightarrow \tau e$ rates, together with a set of observables that we find to be the most constraining ones, and we will conclude that sizable rates of up to 2×10^{-7} , accessible at future colliders, can be reached in this model for Majorana masses in the few TeV range, potentially reachable at LHC.

DOI: [10.1103/PhysRevD.95.075028](https://doi.org/10.1103/PhysRevD.95.075028)

I. INTRODUCTION

The observation of neutrino oscillations, showing that neutrinos do have masses and that lepton flavor violation (LFV) occurs in the neutrino sector, is at present the clearest experimental evidence that the Standard Model (SM) of particle physics is insufficient to explain data and needs to be extended. However, what is the particular new physics responsible for giving mass to the neutrinos and what is the origin of the neutrino flavor oscillations are still open questions that need to be answered. The minimal *ad hoc* extension would be the addition of right-handed (RH) neutrino fields, ν_R , to the SM spectrum, so that neutrinos could obtain a Dirac mass through their Yukawa interaction with the Higgs field, as the rest of the SM fermions. Nevertheless, this requires very small neutrino Yukawa couplings and an additional explanation of why there is not a Majorana mass term for the ν_R fields, since they are singlets under the full SM gauge group. One of the most popular extensions that tries to address these questions is the type-I seesaw model [1–5] that adds RH neutrinos to the SM spectrum, allows both Dirac and heavy Majorana masses for the neutrinos, and explains the smallness of the experimentally observed light neutrino masses in terms of the small ratio of two very distant mass scales, the Dirac mass and the Majorana mass. This condition demands either a tiny neutrino Yukawa coupling or an extremely heavy Majorana mass scale, of the order of 10^{14-15} GeV. Thus, in these high scale seesaw models the differences in their phenomenological predictions with

respect to the SM ones, due to the presence of the new very heavy neutrinos, are in general extremely suppressed [6–8]. In contrast, it is well known that this suppression may be alleviated in low scale seesaw models, where the seesaw scale providing the mass to the heavy neutrinos can be successfully set to much lower values, even reachable at present colliders, like the CERN-LHC. These low scale seesaw models are variants of the type-I seesaw model where the smallness of the light neutrinos and the total lepton number (LN) symmetry are controlled instead by some additional small mass parameters. By the use of symmetry arguments that preserve the small size of these new mass parameters the low scale seesaw models then leave the possibility to lower the heavy neutrino mass scale, below 10 TeV, while keeping at the same time an interesting phenomenology due to the allowed presence of large neutrino Yukawa couplings.

On the other hand, one of the most interesting aspects of these low scale seesaw models is that the associated extension of the neutral lepton sector may also induce new rare phenomena in the charged lepton sector. In particular, any observation of lepton flavor violation in the charged lepton sector (cLFV) would automatically imply the presence of new physics beyond the SM and could help throwing light on the question of what is the mechanism that generates the neutrino masses. Although cLFV has not been observed yet in nature, there is an extensive experimental program developing different strategies to look for new physics signals in this charged lepton sector and, indeed, there are already at present very competitive upper bounds on several cLFV processes. We summarize some of the current upper bounds on cLFV transitions in Table I and the corresponding ones to the LFV Z gauge boson decays (LFVZD) and LFV H

^{*}valentina.deromeri@uam.es

[†]maria.herrero@uam.es

[‡]xabier.marcano@uam.es

[§]francesca.scarcella@studio.unibo.it

TABLE I. Present upper bounds and future expected sensitivities for cLFV transitions.

LFV observable	Present bound (90% C.L.)	Future sensitivity
$\text{BR}(\mu \rightarrow e\gamma)$	4.2×10^{-13} (MEG 2016)[24]	4×10^{-14} (MEG-II) [25]
$\text{BR}(\tau \rightarrow e\gamma)$	3.3×10^{-8} (BABAR 2010) [26]	10^{-9} (BELLE-II) [27]
$\text{BR}(\tau \rightarrow \mu\gamma)$	4.4×10^{-8} (BABAR 2010) [26]	10^{-9} (BELLE-II) [27]
$\text{BR}(\mu \rightarrow eee)$	1.0×10^{-12} (SINDRUM 1988) [28]	10^{-16} Mu3E (PSI) [29]
$\text{BR}(\tau \rightarrow eee)$	2.7×10^{-8} (BELLE 2010) [30]	$10^{-9,-10}$ (BELLE-II) [27]
$\text{BR}(\tau \rightarrow \mu\mu\mu)$	2.1×10^{-8} (BELLE 2010) [30]	$10^{-9,-10}$ (BELLE-II) [27]
$\text{BR}(\tau \rightarrow \mu\eta)$	2.3×10^{-8} (BELLE 2010) [31]	$10^{-9,-10}$ (BELLE-II) [27]
$\text{CR}(\mu - e, \text{Au})$	7.0×10^{-13} (SINDRUM II 2006) [32]	
$\text{CR}(\mu - e, \text{Ti})$	4.3×10^{-12} (SINDRUM II 2004) [33]	10^{-18} PRISM (J-PARC) [34]
$\text{CR}(\mu - e, \text{Al})$		3.1×10^{-15} COMET-I (J-PARC) [35]
		2.6×10^{-17} COMET-II (J-PARC) [35]
		2.5×10^{-17} Mu2E (Fermilab) [36]

boson decays in Table II. It is interesting to notice that the LHC is currently improving notably these two latter bounds and that ATLAS is already at the level of LEP results for the LFVZD rates, and even better for $Z \rightarrow \mu e$ [9]. Furthermore, the sensitivity to LFVZD rates are expected to highly improve at future linear colliders, with an expected sensitivity of 10^{-9} [10,11], or at a future circular e^+e^- collider (such as FCC-ee [12]), where it is estimated that up to 10^{13} Z bosons would be produced and the sensitivities to LFVZD rates could be improved up to 10^{-13} . Therefore, we consider it extremely timely to explore the predictions for these LFVZD rates in any new physics scenario that could be related to neutrino physics, as has been previously done in beyond the Standard Model frameworks such as those with massive (Majorana and/or Dirac) neutrinos [6,13–19], or those using an effective field theory approach [20–23].

In this work, we consider the inverse seesaw (ISS) [14,42–44] as a specific realization of the low scale seesaw models. In particular, the ISS extends the SM spectrum with three pairs of RH neutrinos with opposite lepton numbers and considers Majorana masses for some of these new fields, which are assumed to be naturally small since they are the only masses that violate LN. Generically, these small Majorana masses are responsible for explaining the smallness of the light neutrino masses and give the freedom

of having simultaneously large Yukawa couplings and moderately heavy RH neutrino masses, reachable at LHC, while keeping the values of the light neutrino masses and mixings in agreement with experimental data. These features make the ISS an appealing model with a very rich phenomenology that has been studied in various processes like leptonic and semileptonic decays [45,46], electric dipole moments [47,48], lepton magnetic moments [49], heavy neutrino production at colliders [50–56], dark matter [57], LFV Higgs decays [58,59], and many other cLFV processes [60–62]. Nevertheless, looking at the present experimental upper bounds in Table I, we see that the constraints on cLFV processes involving μ - e transitions, here called $\text{LFV}_{\mu e}$ in short, are much stronger than the ones in the other sectors, i.e., cLFV processes involving τ - μ and τ - e transitions, named here in short $\text{LFV}_{\tau\mu}$ and $\text{LFV}_{\tau e}$, respectively. These very stringent constraints in the μ - e sector motivate the class of models considered here, which incorporate automatically this suppression in their input. Specifically, we will implement this μ - e suppression requirement within the context of the ISS, by working with the same kind of scenarios that were previously proposed in Refs. [54,58,59]. On the other hand, these particular ISS settings with suppressed $\text{LFV}_{\mu e}$ rates provide very interesting scenarios for exploring the relevant ISS

TABLE II. Present upper bounds at 95% C.L. on LFV decays of Z and H bosons.

LFV observable	Present bound (95% C.L.)
$\text{BR}(Z \rightarrow \mu e)$	1.7×10^{-6} (LEP 1995) [37], 7.5×10^{-7} (ATLAS 2014) [9]
$\text{BR}(Z \rightarrow \tau e)$	9.8×10^{-6} (LEP 1995) [37]
$\text{BR}(Z \rightarrow \tau\mu)$	1.2×10^{-5} (LEP 1995) [38], 1.69×10^{-5} (ATLAS 2014) [39]
$\text{BR}(H \rightarrow \mu e)$	3.6×10^{-3} (CMS 2015) [40]
$\text{BR}(H \rightarrow \tau e)$	1.04×10^{-2} (ATLAS 2016) [39], 0.7×10^{-2} (CMS 2015) [40]
$\text{BR}(H \rightarrow \tau\mu)$	1.43×10^{-2} (ATLAS 2016) [39], 1.51×10^{-2} (CMS 2015) [41]

parameter space directions that may lead to large cLFV rates in the other sectors, τ - μ and/or τ - e .

Motivated by all the peculiarities exposed above, in this work we perform a dedicated study of the LFVZD rates, in particular $\text{BR}(Z \rightarrow \tau\mu)$ and $\text{BR}(Z \rightarrow \tau e)$, in the context of these ISS scenarios with an *ad hoc* suppression of $\text{LFV}_{\mu e}$ rates, which will be called from now on ISS-LFV $_{\mu e}$ in short. LFVZD processes in the presence of low scale heavy neutrinos have recently been studied considering the full one-loop contributions [63] or computing the relevant Wilson coefficients [64]. In these works, maximum allowed LFVZD rates in the reach of future linear colliders were found when considering a minimal “3 + 1” toy model, with $\text{BR}(Z \rightarrow \tau\mu)$ up to $\mathcal{O}(10^{-8})$ for a neutrino mass in the few TeV range. For more realistic models, such as the (2,3) or (3,3) realizations of the ISS model, and after imposing all the relevant theoretical and experimental bounds, smaller LFVZD rates were achieved, $\text{BR}(Z \rightarrow \tau\mu) \lesssim \mathcal{O}(10^{-9})$, which would be below the reach of future linear colliders sensitivities and might be accessible only at future circular e^+e^- colliders. The main difference of our study with the ones previously done relies on the different settings of the ISS parameters, as we will focus on some specific directions that are more difficult to access with a random scan of the ISS parameter space. In the present paper, we will perform a complementary analysis to the one in Ref. [63], and we will show that larger maximum allowed rates for $\text{BR}(Z \rightarrow \tau\mu)$ and $\text{BR}(Z \rightarrow \tau e)$ can be obtained by considering the particular ISS-LFV $_{\mu e}$ scenarios previously commented, such that for some specific directions of the parameter space they could be reached at future linear colliders.

This work is organized as follows. In Sec. II we briefly review the main features of the ISS model and describe in detail our geometrical parametrization of the neutrino Yukawa matrix that allows us to find the scenarios with suppressed $\text{LFV}_{\mu e}$ that we are interested in. We first analyze in Sec. III the behavior of the most relevant constraining observables to the LFVZD rates in terms of the relevant parameters in these peculiar scenarios. Then we devote Sec. IV to present our numerical results for the LFVZD rates in this ISS-LFV $_{\mu e}$ model, and we find out the maximum allowed $\text{BR}(Z \rightarrow \tau\mu)$ and $\text{BR}(Z \rightarrow \tau e)$ rates being compatible with all the relevant experimental and theoretical constraints. Finally, we conclude in Sec. V.

II. THE ISS MODEL WITH SUPPRESSED μ - e TRANSITIONS

We consider a realization of the ISS where three pairs of fermionic singlets, (ν_R, X) , with opposite LN are added to the SM particle content and assume, as usual in this model, that LN is almost conserved, slightly broken only by a small Majorana mass term for the X singlets. This small scale μ_X will be, precisely, responsible for explaining the

smallness of the light neutrino masses. Apart from this Majorana mass term, the rest of the ISS Lagrangian terms conserve LN, and these are the Yukawa interactions between the right- and left-handed neutrinos, ν_R and ν_L , and a mass term connecting the two fermionic singlets ν_R and X . Therefore, we extend the SM Lagrangian with the following terms:

$$\mathcal{L}_{\text{ISS}} = -Y_\nu^{ij} \bar{L}_i \tilde{\Phi} \nu_{Rj} - M_R^{ij} \bar{\nu}_{Ri}^c X_j - \frac{1}{2} \mu_X^{ij} \bar{X}_i^c X_j + \text{H.c.}, \quad (1)$$

where the indices i, j run from 1 to 3, L is the SM lepton doublet, $\tilde{\Phi} = i\sigma_2 \Phi^*$ with Φ the SM Higgs doublet, Y_ν is the 3×3 neutrino Yukawa coupling matrix, M_R is a LN conserving complex 3×3 mass matrix, and μ_X is a Majorana complex 3×3 symmetric mass matrix that violates LN by two units. It is worth mentioning that it is possible to add in Eq. (1) another LN violating Majorana mass term for the ν_R fields, i.e., $\mu_R^{ij} \bar{\nu}_{Ri}^c \nu_{Rj}$ with μ_R a 3×3 symmetric matrix. Assuming this μ_R Majorana scale to be small, the new term will respect the approximated LN symmetry required by the ISS. Nevertheless, μ_R does not generate light neutrino masses at tree level, whereas the Majorana mass μ_X does. The effects of this Majorana mass term for ν_R appear only at one-loop level in the light neutrino masses. Furthermore, the effects of the tiny Majorana mass terms for both ν_R and X fields are negligible for the LFV Z decays studied in this work, which are governed by the Yukawa couplings. Therefore, we will set μ_R to zero for the rest of this work and consider a small μ_X as the only lepton number violating parameter leading to the light neutrino masses.

After the electroweak symmetry breaking has taken place, the following 9×9 neutrino mass matrix is obtained in the (ν_L^c, ν_R, X) basis:

$$M_{\text{ISS}} = \begin{pmatrix} 0 & m_D & 0 \\ m_D^T & 0 & M_R \\ 0 & M_R^T & \mu_X \end{pmatrix}, \quad (2)$$

where the Dirac mass matrix is defined as $m_D = vY_\nu$, with $v = \langle \phi \rangle = 174$ GeV. This 9×9 symmetric mass matrix can be diagonalized by a unitary matrix U^ν , leading to nine physical Majorana states $n_j (j = 1, \dots, 9)$ with masses given by

$$U^{\nu T} M_{\text{ISS}} U^\nu = \text{diag}(m_{n_1}, \dots, m_{n_9}). \quad (3)$$

For completeness, we summarize the relevant neutrino interactions for the observables studied here, i.e., the ones to the W and Z gauge bosons, to the Higgs boson H , and to the Goldstone bosons G . In the neutrino mass basis, they are given by the following terms in the Lagrangian:

$$\mathcal{L}_W = -\frac{g}{\sqrt{2}} \sum_{i=1}^3 \sum_{j=1}^9 W_\mu^- \bar{\ell}_i B_{\ell_i n_j} \gamma^\mu P_L n_j + \text{H.c.}, \quad (4)$$

$$\mathcal{L}_Z = -\frac{g}{4c_W} \sum_{i,j=1}^9 Z_\mu \bar{n}_i \gamma^\mu [C_{n_i n_j} P_L - C_{n_i n_j}^* P_R] n_j, \quad (5)$$

$$\mathcal{L}_H = -\frac{g}{2m_W} \sum_{i,j=1}^9 H \bar{n}_i C_{n_i n_j} [m_{n_i} P_L + m_{n_j} P_R] n_j, \quad (6)$$

$$\mathcal{L}_{G^\pm} = -\frac{g}{\sqrt{2}m_W} \sum_{i=1}^3 \sum_{j=1}^9 G^\pm \bar{\ell}_i B_{\ell_i n_j} [m_{\ell_i} P_L - m_{n_j} P_R] n_j + \text{H.c.}, \quad (7)$$

$$\mathcal{L}_{G^0} = -\frac{ig}{2m_W} \sum_{i,j=1}^9 G^0 \bar{n}_i C_{n_i n_j} [m_{n_i} P_L - m_{n_j} P_R] n_j, \quad (8)$$

where

$$B_{\ell_i n_j} = U_{ij}^{*\nu}, \quad (9)$$

$$C_{n_i n_j} = \sum_{k=1}^3 U_{ki}^\nu U_{kj}^{*\nu}, \quad (10)$$

and $P_{R,L} = (1 \pm \gamma^5)/2$ are the usual chirality projectors. The charged leptons are assumed to be in the physical basis in all this work.

As mentioned above, we assume that μ_X is much smaller than the other masses m_D and M_R . In this situation, six of the physical states, $n_{4,\dots,9}$, are heavy Majorana neutrinos, named here as $N_{1,\dots,6}$, which can be grouped into three pseudo-Dirac pairs with nearly degenerate masses within each pair. The other three states, $n_{1,2,3}$, are light Majorana fermions with masses proportional to μ_X , which are therefore identified as the light neutrinos, $\nu_{1,2,3}$, measured in the oscillation experiments. The small differences among the two quasidegenerate heavy neutrino masses in each pair are also governed by the mass parameter μ_X . The corresponding pairings of these heavy neutrinos are denoted here as $N_{1/2}$, $N_{3/4}$, and $N_{5/6}$, with $m_{N_{1/2}} \leq m_{N_{2/3}} \leq m_{N_{5/6}}$. Generically, the behavior with μ_X , m_D , and M_R of the predicted light and heavy neutrino masses in this ISS model with nine Majorana neutrinos follow a similar pattern as in the one generation case, where the light ν and the two heavy neutrinos $N_{a/b}$ in the unique pseudo-Dirac pair have masses, for $\mu_X \ll m_D, M_R$, given by

$$m_\nu = \frac{m_D^2}{m_D^2 + M_R^2} \mu_X, \quad (11)$$

$$m_{N_{a/b}} = \pm \sqrt{M_R^2 + m_D^2} + \frac{M_R^2 \mu_X}{2(m_D^2 + M_R^2)}. \quad (12)$$

Furthermore, assuming the mass hierarchy $\mu_X \ll m_D \ll M_R$, the masses of the three heavy pairs are dominated by M_R , and the low energy neutrino data can easily be accommodated by using the μ_X parametrization introduced in Ref. [58],

$$\mu_X = M_R^T m_D^{-1} U_{\text{PMNS}}^* m_\nu U_{\text{PMNS}}^\dagger m_D^{T-1} M_R, \quad (13)$$

where $m_\nu = \text{diag}(m_{\nu_1}, m_{\nu_2}, m_{\nu_3})$ are the masses of the three lightest neutrinos and U_{PMNS} is the Pontecorvo-Maki-Nakagawa-Sakata (PMNS) unitary matrix [65,66]. The main advantage of using this parametrization is that it allows us to consider the heavy neutrino mass matrix M_R and the Yukawa coupling matrix as our input parameters for the ISS model. For the numerical estimates, unless otherwise specified, we will consider a normal mass ordering for the light neutrinos with the lightest neutrino mass fixed at $m_{\nu_1} = 0.01$ eV, and the rest of the masses and mixing angles set to their central values of the global fit [67],

$$\begin{aligned} \sin^2 \theta_{12} &= 0.308_{-0.012}^{+0.013}, & \Delta m_{21}^2 &= 7.49_{-0.17}^{+0.19} \times 10^{-5} \text{ eV}^2, \\ \sin^2 \theta_{23} &= 0.574_{-0.144}^{+0.026}, & \Delta m_{31}^2 &= 2.484_{-0.048}^{+0.045} \times 10^{-3} \text{ eV}^2, \\ \sin^2 \theta_{13} &= 0.0217_{-0.0010}^{+0.0013}. \end{aligned} \quad (14)$$

For the rest of this paper, we work in the basis where M_R is diagonal and assume the simplest case where all its entries are degenerate and real, i.e., $M_{R_{1,2,3}} \equiv M_R$. In order to avoid potential constraints from lepton electric dipole moments, we also consider only real values for the Y_ν matrix, as well as for the PMNS matrix. In this situation, the one-loop induced cLFV processes are driven by powers of the combination $Y_\nu Y_\nu^T$, instead of $Y_\nu Y_\nu^\dagger$, and it turns out to be useful and instructive to apply the geometrical interpretation discussed in [58], where the nine entries of the Yukawa matrix are interpreted in terms of the components of three generic neutrino vectors in flavor space ($\mathbf{n}_e, \mathbf{n}_\mu, \mathbf{n}_\tau$),

$$Y_\nu = \begin{pmatrix} Y_{\nu_{11}} & Y_{\nu_{12}} & Y_{\nu_{13}} \\ Y_{\nu_{21}} & Y_{\nu_{22}} & Y_{\nu_{23}} \\ Y_{\nu_{31}} & Y_{\nu_{32}} & Y_{\nu_{33}} \end{pmatrix} \equiv f \begin{pmatrix} \mathbf{n}_e \\ \mathbf{n}_\mu \\ \mathbf{n}_\tau \end{pmatrix}, \quad (15)$$

which for the relevant combination in cLFV processes give

$$Y_\nu Y_\nu^T = f^2 \begin{pmatrix} |\mathbf{n}_e|^2 & \mathbf{n}_e \cdot \mathbf{n}_\mu & \mathbf{n}_e \cdot \mathbf{n}_\tau \\ \mathbf{n}_e \cdot \mathbf{n}_\mu & |\mathbf{n}_\mu|^2 & \mathbf{n}_\mu \cdot \mathbf{n}_\tau \\ \mathbf{n}_e \cdot \mathbf{n}_\tau & \mathbf{n}_\mu \cdot \mathbf{n}_\tau & |\mathbf{n}_\tau|^2 \end{pmatrix}. \quad (16)$$

This means that the input parameters that determine the Y_ν matrix can be seen as the three modulus of these three vectors ($|\mathbf{n}_e|, |\mathbf{n}_\mu|, |\mathbf{n}_\tau|$), the three relative *flavor* angles between them ($\theta_{\mu e}, \theta_{\tau e}, \theta_{\tau \mu}$), with $\theta_{ij} \equiv \widehat{\mathbf{n}_i \cdot \mathbf{n}_j}$, and three extra angles ($\theta_1, \theta_2, \theta_3$) that parametrize a global rotation \mathcal{O}

of these three vectors that does not change their relative angles. In addition, we have introduced the parameter f that characterizes the global Yukawa coupling strength. Since the combination $Y_\nu Y_\nu^T / f^2$ is symmetric, it only depends on six parameters that we take to be the three modulus ($|\mathbf{n}_e|, |\mathbf{n}_\mu|, |\mathbf{n}_\tau|$) and the cosine of the three flavor angles ($c_{\mu e}, c_{\tau e}, c_{\tau\mu}$), with $c_{ij} \equiv \cos \theta_{ij}$. The names of the angles are motivated by the fact that the cosine of the angle θ_{ij} controls the LFV transitions in the ℓ_i - ℓ_j sector, which we write in short as LFV $_{\ell_i \ell_j}$. It is interesting to notice that the global rotation \mathcal{O} does not enter in the $Y_\nu Y_\nu^T$ combination and, therefore, it will not affect any of the cLFV processes studied in this work.

As mentioned in the Introduction, experimental searches in Table I indicate that the existence of LFV in the μ - e sector is by far much more constrained than in the other τ - μ and τ - e sectors. Therefore, and leaving apart the issue of which could be the theoretical origin of these remarkable differences among the transitions of the various sectors, it may suggest indeed a realistic absence of LFV transitions in the μ - e sector in nature, motivating the study of models that incorporate these peculiarities automatically in their input settings. In particular, the μ - e suppression can be easily realized with our geometrical interpretation by just assuming that \mathbf{n}_e and \mathbf{n}_μ are orthogonal vectors, i.e., $c_{\mu e} = 0$. Such a condition defines a family of ISS scenarios that can be parametrized using the following Yukawa matrix:

$$Y_\nu = A \cdot \mathcal{O} \quad \text{with} \quad A \equiv f \begin{pmatrix} |\mathbf{n}_e| & 0 & 0 \\ 0 & |\mathbf{n}_\mu| & 0 \\ |\mathbf{n}_\tau| c_{\tau e} & |\mathbf{n}_\tau| c_{\tau\mu} & |\mathbf{n}_\tau| \sqrt{1 - c_{\tau e}^2 - c_{\tau\mu}^2} \end{pmatrix}, \quad (17)$$

where \mathcal{O} is the above commented orthogonal rotation matrix, which does not enter in the product $Y_\nu Y_\nu^T$, and we have factorized out again the parameter f that controls the global strength of the Yukawa coupling matrix. Notice that the Y_ν matrix in Eq. (17) is the most general one that satisfies the condition $c_{\mu e} = 0$.

In order to better understand the implications on cLFV phenomenology of these ISS scenarios, we first explore in this section the LFV radiative decays that, as we have said, are one of the most constrained cLFV observables. All the numerical estimates and plots in this work are made using the full one-loop formulas of the radiative decays in the neutrino mass basis [6], which are provided in Appendix A for completeness. Nevertheless, for the purpose of the following discussion, it proves convenient to comment first on the dependence of the relevant parameters by using the following approximate expression—which is very simple and has been proven to work quite well in the present ISS context [58], as long as $vY_\nu \ll M_R$:

$$\text{BR}(\ell_m \rightarrow \ell_k \gamma) \approx \frac{\alpha_W^3 s_W^2}{1024 \pi^2 m_W^4} \frac{m_{\ell_m}^5 v^4}{\Gamma_{\ell_m} M_R^4} |(Y_\nu Y_\nu^T)_{km}|^2. \quad (18)$$

From this equation, we can easily see that the LFV radiative decays of the τ lepton depend on the most relevant parameters, f , M_R , and $c_{\tau\ell}$ as follows:

$$\text{BR}(\tau \rightarrow \ell \gamma) \sim \frac{f^4}{M_R^4} c_{\tau\ell}^2 \quad \text{with} \quad \ell = e, \mu. \quad (19)$$

The case of $\mu \rightarrow e \gamma$ is different, since the assumption $c_{\mu e} = 0$ cancels the leading order contribution given by the approximate formula in Eq. (18), so the first relevant contribution in this observable is of higher order in the expansion series in powers of the Yukawa coupling. Specifically it is of the type $(Y_\nu Y_\nu^T Y_\nu Y_\nu^T)$. Consequently, it is suppressed with respect to Eq. (19), and the predicted rates for this relevant contribution turn out to depend on the product of both $c_{\tau e}$ and $c_{\tau\mu}$,

$$\text{BR}(\mu \rightarrow e \gamma) \sim \frac{f^8}{M_R^8} c_{\tau e}^2 c_{\tau\mu}^2. \quad (20)$$

Therefore, to get a nonzero value of this $\text{BR}(\mu \rightarrow e \gamma)$ one needs the other two parameters $c_{\tau e}$ and $c_{\tau\mu}$, triggering the respective radiative decays $\tau \rightarrow \mu \gamma$ and $\tau \rightarrow e \gamma$, to be nonvanishing simultaneously.

This generic suppression of the $\text{BR}(\mu \rightarrow e \gamma)$ rates is also illustrated numerically in Fig. 1. This plot shows the full one-loop numerical results for $\text{BR}(\mu \rightarrow e \gamma)$, computed with the complete formulas in Appendix A, and displays the above commented correlations with the corresponding full one-loop predictions of $\text{BR}(\tau \rightarrow \mu \gamma)$ and $\text{BR}(\tau \rightarrow e \gamma)$ via the parameters $c_{\tau\mu}$ and $c_{\tau e}$, respectively. The contour lines for $\text{BR}(\mu \rightarrow e \gamma)$ are obtained by varying $c_{\tau\mu}^2$ and $c_{\tau e}^2$ within the interval (0,0.6), which in turn provide predictions for $\text{BR}(\tau \rightarrow \mu \gamma)$ and $\text{BR}(\tau \rightarrow e \gamma)$ that are represented in the vertical and horizontal axes, respectively. This is for the simple case with $|\mathbf{n}_{e,\mu,\tau}| = f = 1$, $M_R = 1$ TeV, and $\mathcal{O} = \mathbb{1}$ (remember that the result is independent on the choice of \mathcal{O}), but similar qualitative conclusions can be obtained for other choices of these parameters. Notice that since we are assuming a real nonsingular Yukawa matrix, Eq. (17) imposes the condition $c_{\tau e}^2 + c_{\tau\mu}^2 < 1$, making the yellow area, where $c_{\tau e}^2 + c_{\tau\mu}^2 \geq 1$, not accessible in our analysis. We also find that the rates for $\tau \rightarrow \mu \gamma$ ($\tau \rightarrow e \gamma$) can in general be large, for the values of the parameters selected in this plot, of the order of the present upper bound from BABAR [26], marked here with a green (orange) arrow, and that they depend just on $c_{\tau\mu}^2$ ($c_{\tau e}^2$), in agreement with the approximate expression in Eq. (19). We also learn that the predictions for $\text{BR}(\mu \rightarrow e \gamma)$ are 3–4 orders of magnitude smaller than the τ radiative decay rates, as expected from Eq. (20), but they are still above the upper bound from the

MEG experiment for most of the parameter space. In fact, the MEG bound excludes everything but the area close to the axes. Eventually, the $\text{BR}(\mu \rightarrow e\gamma)$ goes asymptotically to zero when approaching the axes. When lying just on top of these axes, the predictions for $\text{BR}(\mu \rightarrow e\gamma)$ completely vanish [see Eq. (20)], implying that $\text{BR}(\tau \rightarrow e\gamma)$ must be small in order to allow for large $\text{BR}(\tau \rightarrow \mu\gamma)$, and vice versa.

Therefore, we focus our analysis on these two directions in the ISS parameter space with suppressed μ - e transitions, identified with the two axes in Fig. 1, that define our ISS-LFV $_{\mu e}$ model. We then consider two classes of scenarios: the TM scenarios along the LFV $_{\tau\mu}$ axis ($c_{\tau e} = 0$) that may give sizable rates for τ - μ transitions, but always give negligible contributions to LFV $_{\mu e}$ and LFV $_{\tau e}$; and the TE scenarios along the LFV $_{\tau e}$ axis ($c_{\tau\mu} = 0$) that may lead to large rates only for the τ - e transitions. In Table III we list the specific examples that we will use for the numerical estimates of our selected TM scenarios, where we have also included, for comparison, the three particular scenarios that were previously introduced in Ref. [58]. Equivalent examples for the TE scenarios are obtained by exchanging μ and e everywhere in the previous TM scenarios.

Finally, to complete the description of this family of scenarios, we remark that they are built mostly for suppressing the loop generated LFV $_{\mu e}$ processes; therefore each of them could give very different results for other tree

level observables, including those preserving flavor. One example of the latter is the heavy neutrino production in association with a charged lepton of a specific flavor, which can be used to define the flavor of the heavy neutrinos [54]. In Fig. 2 we show the predicted flavor pattern of the six heavy neutrinos, N_i ($i = 1 \dots 6$) grouped in pairs, for our eight selected scenarios TM-1 through TM-8. The length of the colored bars is calculated as

$$S_{\ell N_i} = \frac{|B_{\ell N_i}|^2}{\sum_{\ell=e,\mu,\tau} |B_{\ell N_i}|^2}, \quad (21)$$

and, therefore, represents the relative mixing of the heavy neutrino N_i with a given flavor ℓ . We learn from Fig. 2 that, although all these TM scenarios share the property of suppressing the LFV μ - e and τ - e rates while maximizing the τ - μ ones, the heavy neutrino flavor mixing pattern is different in each scenario. A common feature in almost all scenarios but TM-6 is that there is always one heavy pseudo-Dirac neutrino pair that is dominantly e flavored (the bar filled in blue).

III. OBSERVABLES CONSTRAINING THE LFVZD RATES

As we discussed in the previous section, strong experimental upper bounds on LFV $_{\mu e}$ transitions suggest that sizable LFV rates involving a τ lepton can be achieved just

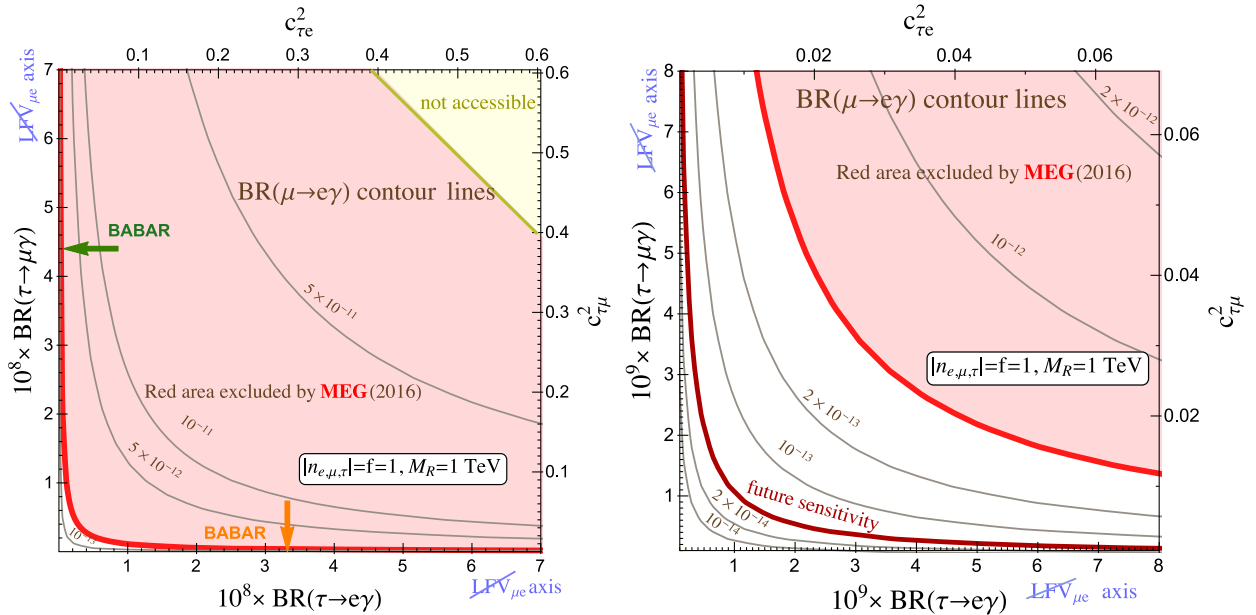


FIG. 1. Left panel: Contour lines for $\text{BR}(\mu \rightarrow e\gamma)$ as a function of $\text{BR}(\tau \rightarrow e\gamma)$ and $\text{BR}(\tau \rightarrow \mu\gamma)$ rates, for fixed $M_R = 1$ TeV, $|n_{e,\mu,\tau}| = f = 1$ values, and varying $c_{\tau e}^2$ and $c_{\tau\mu}^2$ from 0 to 0.6, as shown in the right and top axes. The yellow area represents the region that cannot be accessed with real Yukawa matrices. The red area is excluded by the upper bound on $\mu \rightarrow e\gamma$ of $\text{BR}(4.2 \times 10^{-13})$ from MEG [24], while the orange (green) arrow marks the present upper bound $\text{BR}(\tau \rightarrow e\gamma) < 3.3 \times 10^{-8}$ [$\text{BR}(\tau \rightarrow \mu\gamma) < 4.4 \times 10^{-8}$] from BABAR [26]. Right panel: Zoom on the lower left corner of the plot in the left panel which allows for a better reading of the region allowed by present experimental data. The extra darker red line represents the future expected sensitivity of 4×10^{-14} by MEG-II [25].

TABLE III. Examples of TM scenarios with τ - μ transitions that we consider in the numerical estimates. The cases where Y_ν is defined with \simeq instead of $=$ means that $c_{\tau\mu} = 0.99$ instead of 1 in order to have a nonsingular Y_ν matrix, as required by Eq. (13). Three scenarios, TM-5, TM-6, and TM-7, were previously introduced in Ref. [58] under the names of $Y_{\tau\mu}^{(1)}$, $Y_{\tau\mu}^{(2)}$, and $Y_{\tau\mu}^{(3)}$, respectively. Equivalent scenarios for the TE class are easily obtained by exchanging μ and e in these TM ones.

Scenario name	$c_{\tau\mu}$	$ n_e $	$ n_\mu $	$ n_\tau $	Example
TM-1	$1/\sqrt{2}$	1	1	1	$Y_\nu = f \begin{pmatrix} 1 & 0 & 0 \\ 0 & 1 & 0 \\ 0 & 1/\sqrt{2} & 1/\sqrt{2} \end{pmatrix}$
TM-2	1	1	1	1	$Y_\nu \simeq f \begin{pmatrix} 1 & 0 & 0 \\ 0 & 1 & 0 \\ 0 & 1 & 0 \end{pmatrix}$
TM-3	$1/\sqrt{2}$	0.1	1	1	$Y_\nu = f \begin{pmatrix} 0.1 & 0 & 0 \\ 0 & 1 & 0 \\ 0 & 1/\sqrt{2} & 1/\sqrt{2} \end{pmatrix}$
TM-4	1	0.1	1	1	$Y_\nu \simeq f \begin{pmatrix} 0.1 & 0 & 0 \\ 0 & 1 & 0 \\ 0 & 1 & 0 \end{pmatrix}$
TM-5	1	$\sqrt{2}$	1.7	$\sqrt{3}$	$Y_\nu = f \begin{pmatrix} 0 & 1 & -1 \\ 0.9 & 1 & 1 \\ 1 & 1 & 1 \end{pmatrix}$ ($Y_{\tau\mu}^{(1)}$ in [58])
TM-6	$1/3$	$\sqrt{2}$	$\sqrt{3}$	$\sqrt{3}$	$Y_\nu = f \begin{pmatrix} 0 & 1 & 1 \\ 1 & 1 & -1 \\ -1 & 1 & -1 \end{pmatrix}$ ($Y_{\tau\mu}^{(2)}$ in [58])
TM-7	0.1	$\sqrt{2}$	$\sqrt{3}$	1.1	$Y_\nu = f \begin{pmatrix} 0 & -1 & 1 \\ -1 & 1 & 1 \\ 0.8 & 0.5 & 0.5 \end{pmatrix}$ ($Y_{\tau\mu}^{(3)}$ in [58])
TM-8	1	$1/2$	$1/3$	$1/4$	$Y_\nu \simeq f \begin{pmatrix} 1 & 0 & 0 \\ 0 & 0.5 & 0 \\ 0 & 0.08 & 0.32 \end{pmatrix}$

in some particular directions in the ISS parameter space with μ - e suppression insured, which we have referred to as ISS-LFV $_{\mu e}$ scenarios. Our aim is to study the LFV Z decays (LFVZD) in this kind of scenarios, looking for their maximum rates that are allowed by all the relevant experimental and theoretical constraints. Our searches in these particular directions of the ISS parameter space are in

contrast to the previous analysis of the LFVZD rates done in Ref. [63], where the ISS parameter space was uniformly scanned, making it more difficult to access these peculiar scenarios that give large rates for LFV transitions with τ leptons allowed by all the constraints, including the more stringent ones coming from μ - e transitions. In this section we make our selection for the set of observables

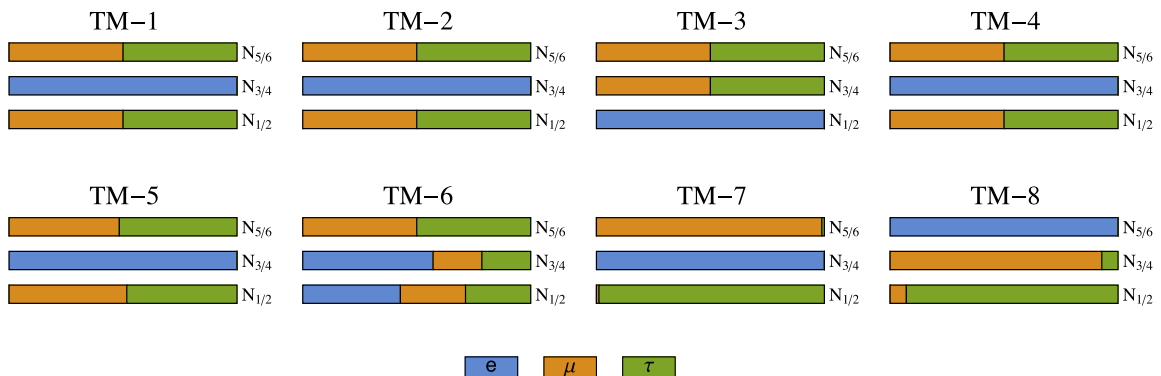


FIG. 2. Heavy neutrino flavor mixings, as defined in Eq. (21), within the ISS scenarios of Table III.

constraining the LFBVD rates which we have checked are the most relevant ones for the present study. We will provide numerical predictions for all the relevant observables in the very specific parameter space directions of the ISS-LFBVD $_{\mu e}$ explored here and compare them directly to their experimental bounds. Alternative checks of the allowed ISS parameter space make use of global fits [68–73], but we prefer to make the explicit computations of the selected observables here in order to focus our search in the optimal directions of our model.

Generically, the addition of heavy Majorana neutrinos to the particle content of the SM has a phenomenological

impact on several observables, including lepton flavor and lepton number violating processes, via their mixing with the active neutrinos. Therefore, we want to ensure that our analysis complies with the relevant theoretical and experimental constraints, in all the regimes of RH neutrino masses considered. We briefly discuss in the following the constraints that we have found to be the most relevant ones for the present work and which we consequently include in our analysis. For this study we have used our own *Mathematica* code which includes all the relevant formulas for the constraining observables that are taken from the literature and that we include in the appendixes for

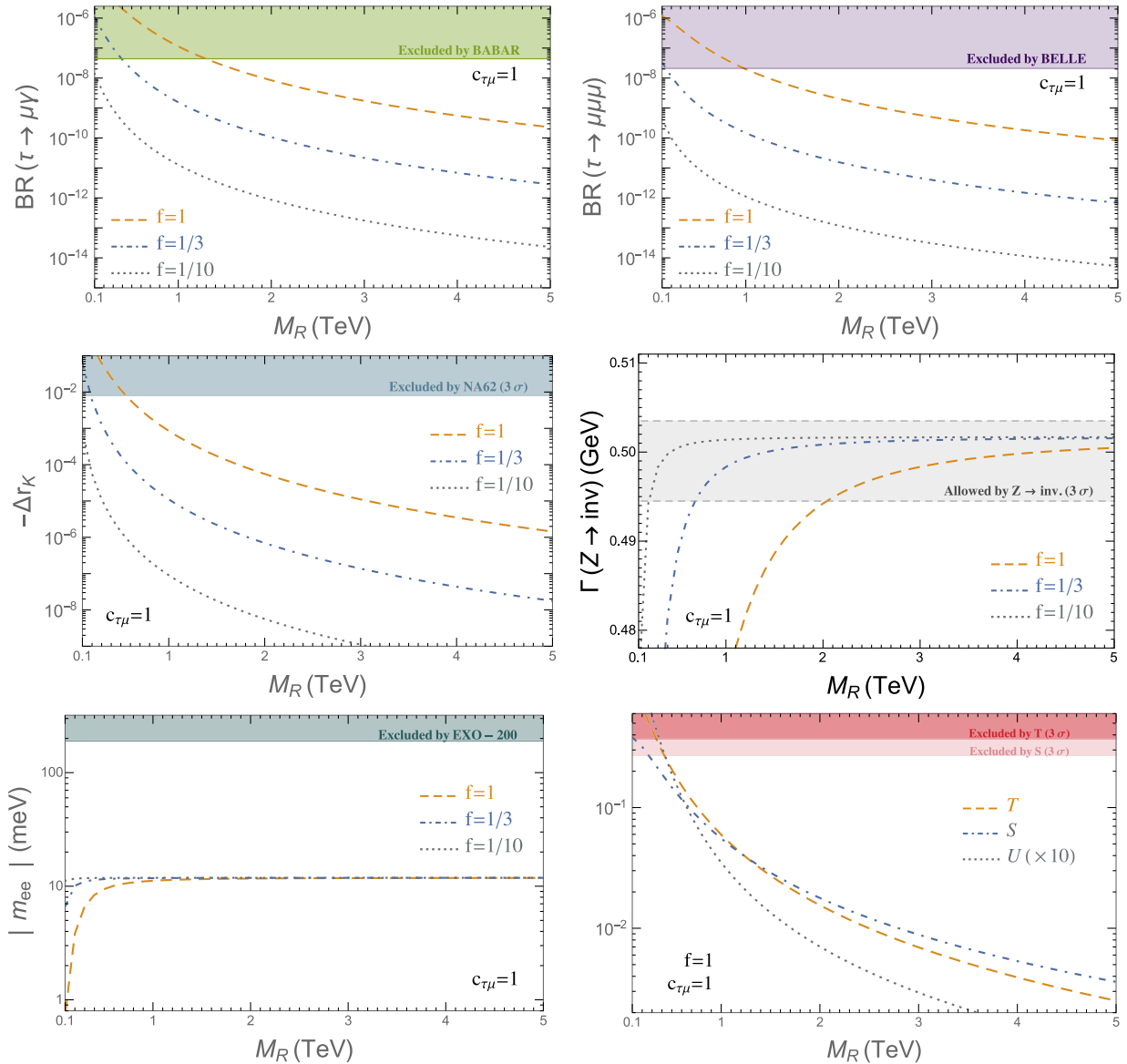


FIG. 3. Predictions for the observables constraining the LFBVD rates as functions of M_R in the ISS. Specifically, from top to bottom and from left to right panels, the corresponding plots are for $\text{BR}(\tau \rightarrow \mu\gamma)$, $\text{BR}(\tau \rightarrow \mu\mu\mu)$, $-\Delta r_k$, $\Gamma(Z \rightarrow \text{inv})$, $|m_{ee}|$, and the electroweak precision parameters S , T , U (the latter enhanced by a factor of 10 to see it more clearly). In all plots we set $|n_{e,\mu,\tau}| = 1$. The upper shadowed bands in all plots, except the Z invisible width, are the excluded regions by present data. For $\Gamma(Z \rightarrow \text{inv})$ the shadowed band is the experimentally allowed region at 3σ sigma level.

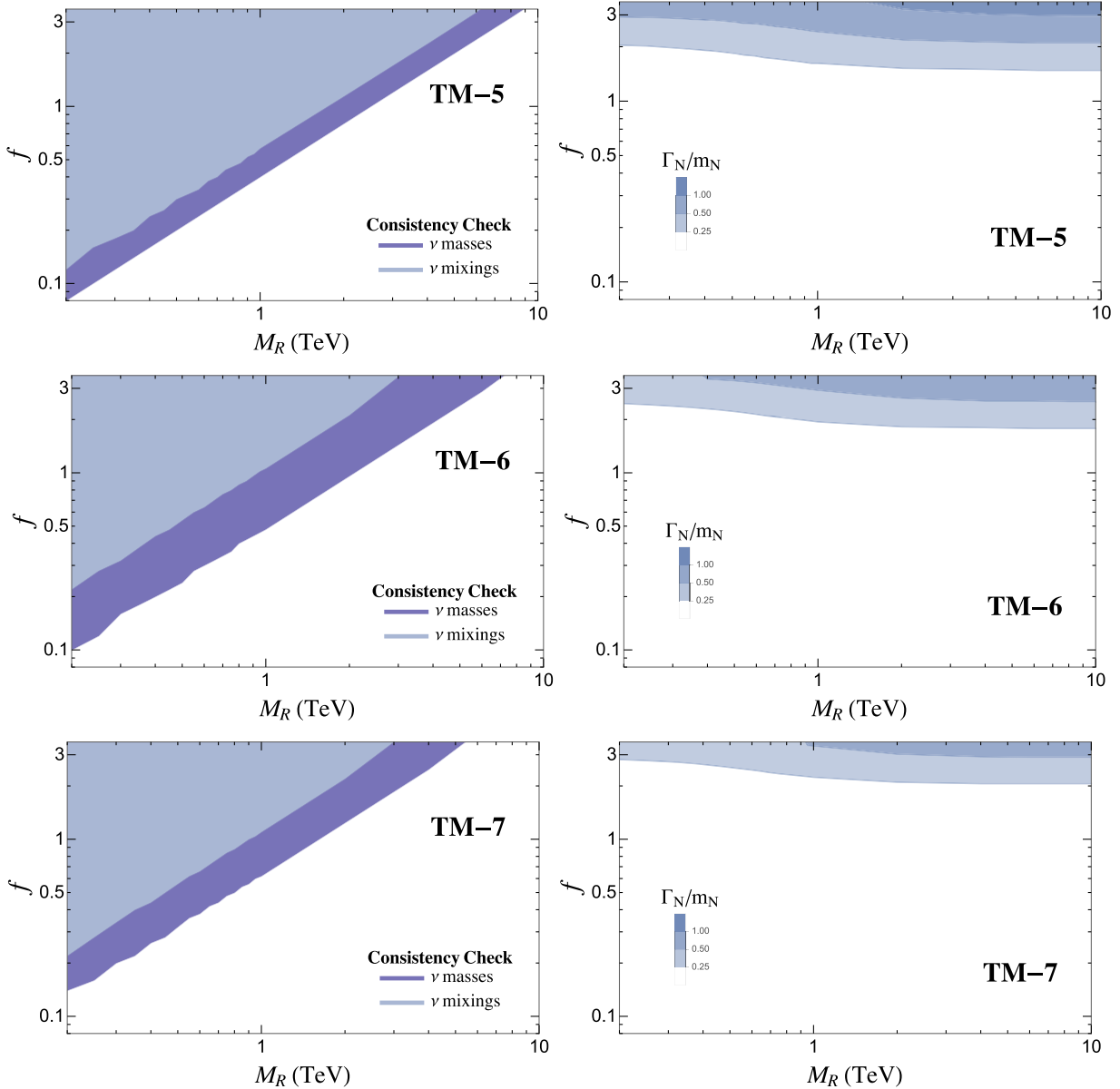


FIG. 4. Theoretical constraints from the requirement of perturbativity (three plots on the right) and from the consistency of the μ_X parametrization (three plots on the left), for the scenarios TM-5, TM-6, and TM-7. The regions excluded by the constraints are the shadowed areas.

completeness. The main numerical results are summarized in Figs. 3 and 4.

A. LFV lepton decays

As mentioned above, there are strong experimental upper bounds on cLFV transitions such as the LFV lepton radiative decays and LFV lepton three body decays. Since, by construction, the ISS-LFV $_{\mu e}$ scenarios that we are studying suppress the LFV in two of the three ℓ_i - ℓ_j sectors, the most relevant LFV constraints are $\tau \rightarrow \mu\gamma$ and $\tau \rightarrow \mu\mu\mu$ for the TM scenarios and $\tau \rightarrow e\gamma$ and $\tau \rightarrow eee$ for the TE scenarios. We compute the rates for these

observables using the full one-loop formulas given in Appendix A that we take from Refs. [6,74] and compare them with their experimental upper limits from *BABAR* and *Belle*, respectively, given in Table I. In the TM scenarios, and equivalently in the TE ones, we find that the rates for these two observables, $\text{BR}(\tau \rightarrow \mu\gamma)$ and $\text{BR}(\tau \rightarrow \mu\mu\mu)$, are independent of $|\mathbf{n}_e|$ and \mathcal{O} , they decouple as expected with M_R and grow with f , $|\mathbf{n}_\mu|$, $|\mathbf{n}_\tau|$, and $c_{\tau\mu}$. The full radiative decays rates indeed follow the behavior of the approximate formula in Eq. (19). In Fig. 3, the predictions for these LFV decays are shown as functions of the two most relevant parameters, M_R and f . We find that for the TM scenarios

with large τ - μ transitions given by $c_{\tau\mu} = 1$, typically, the maximum allowed values for f are $\sim\mathcal{O}(1-0.5)$ for $M_R = 1$ TeV and the minimum allowed values for M_R are $\sim\mathcal{O}(1-2)$ TeV for $f = 1$. We find similar conclusions for the TE scenarios, regarding the $\tau \rightarrow e\gamma$ and $\tau \rightarrow eee$ decays, by simply exchanging μ and e everywhere in the previous TM results.

B. Lepton flavor universality

It has been shown [45,46] that leptonic and semileptonic decays of pseudoscalar mesons (K , D , D_s , B) could also put important constraints on the mixing between the active and the sterile neutrinos in the ISS. In particular, the most severe bounds arise from the violation of lepton universality in leptonic kaon decays.¹ In the following, we will apply this constraint by considering the contributions of the sterile neutrinos to the Δr_k parameter, defined as

$$\Delta r_k = \frac{R_K}{R_K^{\text{SM}}} - 1 \quad \text{with} \quad R_K = \frac{\Gamma(K^+ \rightarrow e^+\nu)}{\Gamma(K^+ \rightarrow \mu^+\nu)}. \quad (22)$$

The comparison of the theoretical calculation in the SM [75,76] with the recent measurements from the NA62 Collaboration [77,78] shows that the experimental measurements agree with the SM prediction within 1σ ,

$$\Delta r_k = (4 \pm 4) \times 10^{-3}. \quad (23)$$

We compute the new physics contributions to Δr_k using the formulas listed in Appendix B that we take from [45], and we apply the bound in Eq. (23) by excluding any solution that falls outside the 3σ region. We have found that the deviations from this band become more important when the ratio between $|\mathbf{n}_e|$ and $|\mathbf{n}_\mu|$ is different from one. Even if in general the constraints on f and M_R that are obtained from this observable are weaker than those obtained from the previous LFV lepton decays, Δr_k turns out to set relevant constraints in some textures—notably TM-7 and TM-8—and in most textures at low M_R .

C. The invisible decay width of the Z boson

The presence of sterile neutrinos affects the tree level predictions of the Z invisible width even if they are above the kinematical threshold, since they modify the couplings of the active neutrinos to the Z boson. The Z invisible decay width was measured in LEP to be [79]

$$\Gamma(Z \rightarrow \text{inv})_{\text{Exp}} = 499 \pm 1.5 \text{ MeV}, \quad (24)$$

¹We do not consider other lepton universality tests in view of the fact that they give similar bounds, as in the case of Δr_k , or they are less constraining, as the ones involving τ leptons [46].

which is about 2σ below the SM prediction,

$$\Gamma(Z \rightarrow \text{inv})_{\text{SM}} = \sum_{\nu} \Gamma(Z \rightarrow \nu\bar{\nu})_{\text{SM}} = 501.69 \pm 0.06 \text{ MeV}. \quad (25)$$

We compute the tree level predictions using the formulas provided in Ref. [46], and we further include the ρ parameter that accounts for the part of the radiative corrections coming from SM loops, i.e.,

$$\Gamma(Z \rightarrow \text{inv})_{\text{ISS}} = \sum_{\substack{i,j=1 \\ i \leq j}}^3 \Gamma(Z \rightarrow n_i n_j)_{\text{ISS}} = \rho \Gamma(Z \rightarrow \text{inv})_{\text{ISS}}^{\text{tree}}, \quad (26)$$

where n_i runs over all kinematically allowed neutrinos and ρ is evaluated as

$$\rho = \frac{\Gamma(Z \rightarrow \text{inv})_{\text{SM}}}{\Gamma(Z \rightarrow \text{inv})_{\text{SM}}^{\text{tree}}}. \quad (27)$$

The analytical formula for the tree level partial width of the Z decay into neutrinos within the ISS is given in Appendix C. We have also estimated the size of the extra loop corrections induced by the new heavy neutrino states using the formulas of Ref. [80] and found out that they are numerically very small compared with the SM loop corrections, so we will neglect them in the following. Moreover, we found that the Z invisible width only depends on M_R , f , and the modulus $|\mathbf{n}_{e,\mu,\tau}|$, while it is not dependent on \mathcal{O} and on the flavor angles ($c_{\tau\mu}$, $c_{\tau e}$), as it was expected, since when adding all the possible neutrino final states in Eq. (26) the dependence on \mathcal{O} and on the flavor angles appearing in each channel disappears in the sum. Regarding the comparison with data we require our predictions to be within the 3σ experimental band [Eq. (24)]. As we can see in Fig. 3, the Z invisible width provides in general quite strong constraints, indeed comparable or even tighter in some cases than the previous constraints from the LFV lepton decays. For instance, for scenarios with $c_{\tau\mu} = 1$ and $f = 1$, this observable also excludes M_R values lower than around 1–2 TeV, similar to the constraints from $\tau \rightarrow \mu\gamma$.

D. Neutrinoless double beta decay

The ISS mechanism calls upon the introduction of singlet neutrinos with Majorana masses, thus allowing for LN violating processes such as neutrinoless double beta decay [81]. Within the ISS framework where six sterile fermions are added to the SM particle content, the effective neutrino mass m_{ee} is given by [49,82,83]

$$\begin{aligned}
m_{ee} &\simeq \sum_{i=1}^9 (B_{en_i})^2 p^2 \frac{m_{n_i}}{p^2 - m_{n_i}^2} \\
&\simeq \left(\sum_{i=1}^3 (B_{en_i})^2 m_{n_i} \right) + p^2 \left(\sum_{i=4}^9 (B_{en_i})^2 \frac{m_{n_i}}{p^2 - m_{n_i}^2} \right),
\end{aligned} \tag{28}$$

where $p^2 \simeq -(125 \text{ MeV})^2$ is an average estimate over different values—depending on the decaying nucleus—of the virtual momentum of the neutrino exchanged in the process.

The neutrinoless double beta decay has not been observed yet by any of the current experiments, actively searching for it. On the other hand, the experiments with highest sensitivity such as GERDA [84], EXO-200 [85,86], and KamLAND-ZEN [87] have allowed one to set strong bounds on the neutrino effective mass. These bounds on the effective neutrino Majorana mass—determining the amplitude of the neutrinoless double beta decay rate—lie in the range

$$|m_{ee}| \lesssim 140 \text{ meV} - 700 \text{ meV}. \tag{29}$$

In our analysis, we apply the most recent constraint from [86], $|m_{ee}| \lesssim 190 \text{ meV}$.

As can be seen in Fig. 3, the maximum value of $|m_{ee}| \sim 10 \text{ meV}$ is reached at large $M_R \gtrsim 1 \text{ TeV}$ and for all studied values of f . We have checked that this asymptotic value depends on the mass of the light active neutrinos, i.e.,

$$m_{\nu_1} \sim 0.01(0.1) \text{ eV} \rightarrow |m_{ee}| \sim 0.01(0.1) \text{ eV}. \tag{30}$$

The overall conclusion is that this observable is much less constraining than the others in what regards our study of LFV Z decay rates.

E. Electroweak precision observables

We take into account constraints from electroweak precision data by computing the S , T , and U parameters [88] and comparing our predictions to the experimental results [79],

$$\begin{aligned}
S &= -0.03 \pm 0.10, & T &= 0.01 \pm 0.12, \\
U &= 0.05 \pm 0.10.
\end{aligned} \tag{31}$$

We use the formulas from Ref. [89] (which we report in Appendix D), and we consider only the parameter space points that give predictions within the 3σ bands. As can be seen in Fig. 3 the constraints on the ISS model from the electroweak precision observables (EWPO), S , T , and U , are in general weaker than from the LFV lepton decays and from the Z invisible width. We have found that the most constraining EWPO is the T parameter and next, although

quite close, the S parameter. For instance, for $f = 1$ and $c_{\tau\mu} = 1$ we find that M_R below around 300 GeV are excluded by T .

F. Perturbativity constraints

In this work, we are considering sizable neutrino Yukawa couplings, so we should check that they are still within the perturbative regime. In order to impose perturbativity either one may choose a direct constraint on the maximum allowed size of the Yukawa matrix entries as, for instance, $|(Y_\nu)_{ij}|^2/(4\pi) < 1$ or, alternatively, one may apply a constraint on an observable that grows with this Yukawa coupling, as it is in the case of the total width of the heavy neutrinos. We choose here this second method and ensure we are considering perturbative couplings by requiring that the total decay width of each heavy neutrino is always less than the corresponding heavy neutrino mass. In particular, we have explored in Fig. 4 the following three assumptions to comply with the perturbative unitary condition:

$$\frac{\Gamma_{N_i}}{m_{N_i}} < 1, \frac{1}{2}, \frac{1}{4} \quad \text{for } i = 1, \dots, 6. \tag{32}$$

Notice that this condition is controlled in our ISS scenarios mainly by the global strength parameter f . Regarding the computation of the total decay width, in the limit $M_R \gg m_D$ that we work with, the possible decay channels are reduced. For $M_R \gg m_D$ the heavy neutrino masses are close to M_R , with small differences of $\mathcal{O}(m_D^2 M_R^{-1})$ between the different pseudo-Dirac pairs and, therefore, assuming they are practically degenerate, their potential decays into other heavy neutrinos are suppressed. In consequence, the dominant decay channels are simply $N_j \rightarrow Z\nu_i, H\nu_i$, and $W^\pm \ell_i^\mp$, and the total neutrino width can easily be computed by adding the corresponding partial widths of these four decays. For instance, the decays into $W^+ \ell_i^-$ or $W^- \ell_i^+$ have a partial width given by

$$\Gamma_{N_j \rightarrow W \ell_i} = \frac{\sqrt{(m_{N_j}^2 - m_{\ell_i}^2 - m_W^2)^2 - 4m_{\ell_i}^2 m_W^2}}{16\pi m_{N_j}^3} |\overline{F}_W|^2, \tag{33}$$

with

$$\begin{aligned}
|\overline{F}_W|^2 &= \frac{g^2}{4m_W^2} |B_{\ell_i N_j}|^2 \\
&\times \{ (m_{N_j}^2 - m_{\ell_i}^2)^2 + m_W^2 (m_{N_j}^2 + m_{\ell_i}^2) - 2m_W^4 \}.
\end{aligned} \tag{34}$$

When summing over all flavors, $i = 1, 2, 3$, in the final state the four ratios turn out to be approximately equal [90],

$$\begin{aligned}
\text{BR}(N_j \rightarrow H\nu) &= \text{BR}(N_j \rightarrow Z\nu) \\
&= \text{BR}(N_j \rightarrow W^+\ell^-) \\
&= \text{BR}(N_j \rightarrow W^-\ell^+) = 25\%. \quad (35)
\end{aligned}$$

In Fig. 4 we show the numerical predictions for the constraints from the perturbativity requirement in three examples of Table III, concretely TM-5, TM-6, and TM-7, and by trying the three choices in Eq. (32). We find that this perturbativity requirement is not much sensitive to M_R , giving an excluded area in the (M_R, f) plane that is a band nearly horizontal and located at the top, which constrains basically just the size of the global Yukawa coupling f , in the most restricted scenarios, to be below order 2–3. In the following, we will take the second choice, 1/2, in Eq. (32) as our constraining condition.

G. Constraints from the μ_X parametrization

As explained in Sec. I, we are using the μ_X parametrization of Eq. (13) to accommodate light neutrino data. In order to check the validity of this parametrization, we require that both the predicted light neutrino mass squared differences and the neutrino mixing angles (more specifically, the corresponding entries of the U_ν matrix that refer to the light neutrinos subblock) that we obtain from the diagonalization of the full neutrino mass matrix [Eq. (2)] lie within the 3σ experimental bands [67,91–94]. The predictions for the constraints found in the three examples, TM-5, TM-6, and TM-7 are shown in Fig. 4. As can be seen in this figure, the bounds obtained from the constraints on the active neutrinos squared mass differences are in these three scenarios stronger than the ones from the light neutrino mixing matrix entries. For other scenarios, like TM-8, we have checked that this can be reversed; i.e., the constraints from the neutrino mixings can be stronger than from the neutrino masses. In general, we found that the area in the (M_R, f) parameter space that is allowed by all the experimental bounds studied in the previous sections is also allowed by the consistency checks of the μ_X parametrization, meaning that the parametrization works well for the parameter space allowed by data. Finally, we have also compared the validity of this parametrization for two values of the input lightest neutrino mass, 0.1 eV and 0.01 eV (the chosen value for Fig. 4), and we have concluded that the μ_X parametrization works better for the case with a smaller value of the light neutrino mass.

IV. RESULTS FOR THE LEPTON FLAVOR VIOLATING Z DECAYS

In order to study the LFVZD rates within the ISS-LFV $_{\mu e}$ model, we have taken the full one-loop formulas from Ref. [18] and we have adapted them to this model; i.e., we have rewritten them in terms of the proper physical neutrino masses and couplings that we have specified in Sec. II. We

include these formulas, for completeness, in Appendix E where we have also adapted the loop functions to the usual notation in the literature. The various contributing one-loop diagrams are also displayed in Fig. 8 below, for completeness. We evaluate them numerically with our code and with the help of the *LoopTools* [95] package for *Mathematica*. We focus our analysis on the particular case of $\text{BR}(Z \rightarrow \tau\mu) = \text{BR}(Z \rightarrow \tau\bar{\mu}) + \text{BR}(Z \rightarrow \mu\bar{\tau})$ within the TM scenarios, which are defined by taking $c_{\tau e} = 0$ in Eq. (17). The relevant parameters in this case are M_R , f , $|\mathbf{n}_\tau|$, $|\mathbf{n}_\mu|$, and $c_{\tau\mu}$. Nevertheless, all our conclusions for $\text{BR}(Z \rightarrow \tau\mu)$ in the TM scenarios can be directly translated to $\text{BR}(Z \rightarrow \tau e)$ in the TE scenarios just by replacing $|\mathbf{n}_\mu|$ and $c_{\tau\mu}$ by $|\mathbf{n}_e|$ and $c_{\tau e}$, respectively.

We display in Fig. 5 the behavior of the $\text{BR}(Z \rightarrow \tau\mu)$ rates with the M_R , f , and $c_{\tau\mu}$ parameters for fixed values of $|\mathbf{n}_e| = |\mathbf{n}_\mu| = |\mathbf{n}_\tau| = 1$, $c_{\tau e} = 0$, and $\mathcal{O} = \mathbb{1}$. As can be seen in this figure, our ISS model gives in general large rates for the LFV Z decay rates, indeed close to the upper bound from LEP (and also close to present LHC sensitivity) in the upper left corner of the two upper plots and in the upper right corner of the two lower plots. We also see that the rates decrease with the heavy scale M_R and grow with the Yukawa coupling strength f , as expected. We found this growth to be approximately as f^4 in the low f region and as f^8 in the high f region of the studied interval of this parameter. This suggests that, in contrast to the radiative decays, the two kinds of contributions $Y_\nu Y_\nu^\dagger$ and $Y_\nu Y_\nu^\dagger Y_\nu Y_\nu^\dagger$ participate in this observable.

In the lower right panel, we observe that the rates also grow with $c_{\tau\mu}$, albeit the dependence is milder, approximately as $c_{\tau\mu}^2$. Although not shown here, we have also studied the dependence of the decay rates with the modulus of the vectors, $|\mathbf{n}_i|$, finding that the predictions for $\text{BR}(Z \rightarrow \tau\mu)$ grow with both $|\mathbf{n}_\mu|$ and $|\mathbf{n}_\tau|$, while they are constant with $|\mathbf{n}_e|$, as expected. Finally, we checked that the results do not depend on the global rotation \mathcal{O} , as argued when the parametrization for the Y_ν coupling matrix was motivated.

Before going to the final analysis of the maximum LFV Z decay rates that are allowed by all the constraints, we find it interesting first to compare the predictions of these LFV Z decays with the predictions of the three body LFV lepton decays in our particular ISS scenarios with suppressed μ - e transitions. In the left panel of Fig. 6 we study the behavior of $\text{BR}(\tau \rightarrow \mu\mu\mu)$ with respect to M_R for the scenario TM-5 and fixed value of $f = 1$, displaying separately the total and the contributions from the γ penguin, boxes, and Z penguin. We see that the full contribution is mostly coming from the latter. The fact that the $\text{BR}(\tau \rightarrow \mu\mu\mu)$ rates are dominated by the Z penguin contributions implies a strong correlation between $\tau \rightarrow \mu\mu\mu$ and $Z \rightarrow \tau\mu$, as already found in Ref. [63]. We have also checked in some examples of the ISS parameter space that our numerical predictions of these two observables are in agreement with that reference.

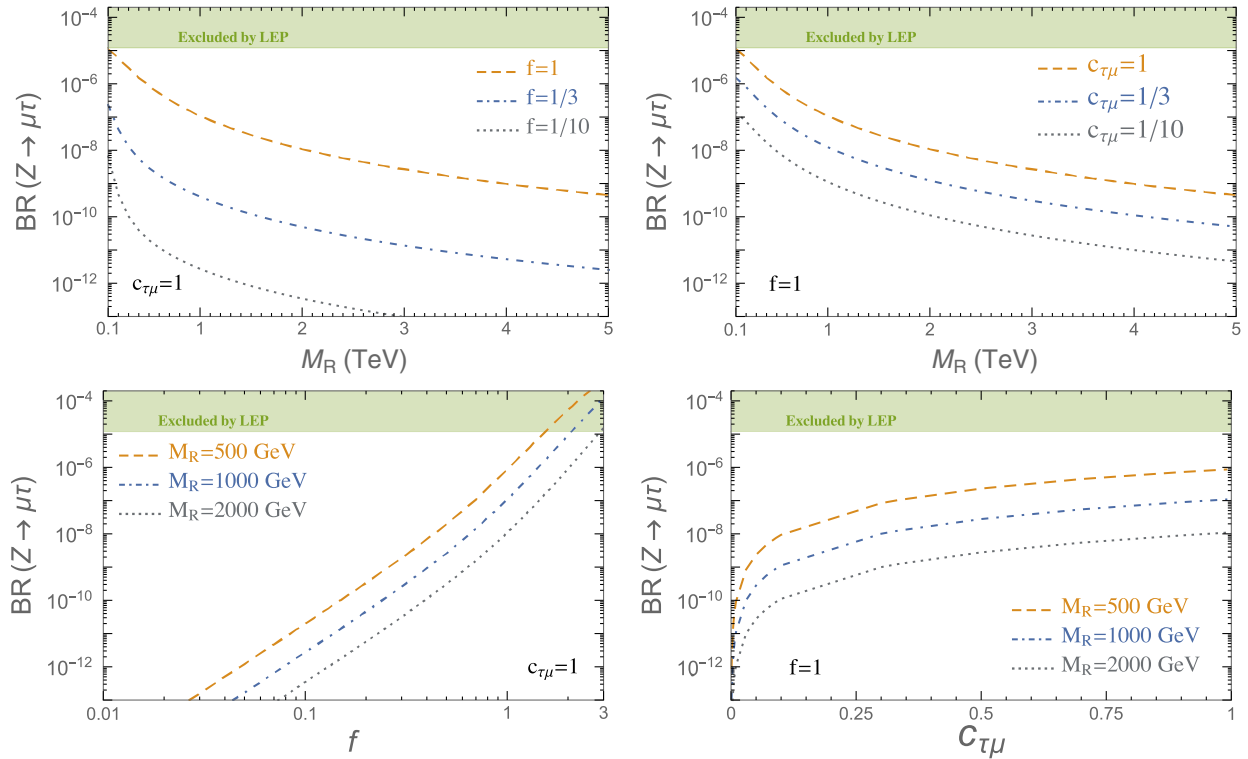


FIG. 5. Predictions for $\text{BR}(Z \rightarrow \tau\mu)$ within the ISS model as a function of the heavy neutrino mass parameter M_R (two upper panels), the neutrino Yukawa coupling strength f (lower left panel), and $c_{\tau\mu}$ (lower right panel) for various choices of the relevant parameters. In all plots we have fixed, $c_{\tau e} = 0$ and $|\mathbf{n}_{e,\mu,\tau}| = 1$. The upper shadowed areas (in green) are excluded by LEP [38]. Similar results for $\text{BR}(Z \rightarrow \tau e)$ by exchanging $c_{\tau e}$ and $c_{\tau\mu}$.

We study this correlation in the right panel of Fig. 6, where we consider three of the scenarios given in Table III, TM-5, TM-6, and TM-7, varying the values of the parameters within the ranges of $f \in (0.1, 2)$ and $M_R \in (0.2, 10)$ TeV. Both observables grow with f and decrease with M_R in approximately the same way, due to

the Z penguin dominance in the three body decays. Although the predicted rates in each scenario are obviously different (see for instance the positions of the reference points with $f = 1$ and $M_R = 3$ TeV), we clearly see that there is a strong correlation between the two observables in our ISS model. We can also conclude from this plot that by

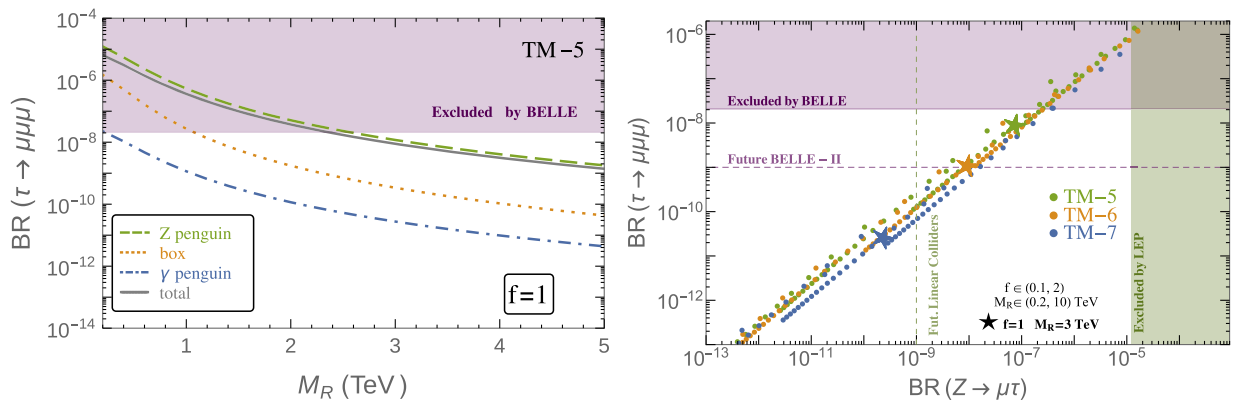


FIG. 6. Left panel: $\text{BR}(\tau \rightarrow \mu\mu\mu)$ as a function of M_R for $f = 1$ in the TM-5 scenario. The full prediction (gray solid line) is decomposed in its contributions from γ penguin (blue dot-dashed line), boxes (yellow dotted line), and Z penguin (green dashed line), the dominant one. Right panel: correlation plot for $\text{BR}(Z \rightarrow \tau\mu)$ and $\text{BR}(\tau \rightarrow \mu\mu\mu)$ for scenarios TM-5 (green dots), TM-6 (yellow dots), and TM-7 (blue dots) defined in Table III. The dots are obtained by varying $f \in (0.1, 2)$ and $M_R \in (0.2, 10)$ TeV, and the stars are for the reference point $f = 1$ and $M_R = 3$ TeV. The purple (green) shadowed area is excluded by Belle [30] (LEP [38]), while the dashed line denotes expected future sensitivity from Belle-II (future linear colliders).

considering just the constraints from the three body decays, i.e., the present upper bound on $\tau \rightarrow \mu\mu\mu$ from Belle, already suggests a maximum allowed rate of $\text{BR}(Z \rightarrow \tau\mu) \sim 2 \times 10^{-7}$, which is clearly within the reach of future linear colliders (10^{-9} in the most conservative option). Interestingly, comparing the future expected sensitivities for both observables, we find some parameter space points where the LFVZD rates are in the reach of future linear colliders while the cLFV three body decay rates would not be accessible in other facilities, like BELLE-II. This fact suggests that experiments looking for LFVZD would be able to provide additional information about the model that complements the results of other searches, like the ones in Table I. We found a similar correlation between $\text{BR}(\tau \rightarrow eee)$ and $\text{BR}(Z \rightarrow \tau e)$ in the TE scenarios.

In the following we present our full analysis of the LFVZD rates in the ISS-LFV $_{\mu e}$, including all the most relevant constraints. For this analysis we have explored the (M_R, f) plane for the eight TM scenarios given in Table III and provide numerical predictions for the $\text{BR}(Z \rightarrow l_i l_j)$ rates together with the predictions of the most constraining observables and their present bounds.

We show in Fig. 7 the results for $\text{BR}(Z \rightarrow \tau\mu)$ together with the constraints from $\tau \rightarrow \mu\mu\mu$, $\tau \rightarrow \mu\gamma$, $Z \rightarrow \text{inv.}$, Δr_K , and the EWPO (S , T , and U). As in the previous section, we show our results only for the LFV $_{\tau\mu}$ sector in the TM scenarios, although the conclusions are very similar for LFV $_{\tau e}$ in the TE scenarios. We use different colors in the shadowed areas to represent the exclusion regions from each of the constraints listed above. Specifically, the purple area is excluded by the upper bound on $\text{BR}(\tau \rightarrow \mu\mu\mu)$, the green area by $\text{BR}(\tau \rightarrow \mu\gamma)$, the yellow area by the Z invisible width, the cyan area by Δr_K , and the area above the pink solid line is excluded by the S , T , U parameters. Although we are not explicitly showing them here, we have also checked that the total parameter space allowed by all these constraints are also permitted by our requirements on perturbativity and on the validity of the μ_X parametrization. Notice that in some scenarios some of the colored areas are hidden below the excluded regions corresponding to the more constraining observables.

On top of all the bounds, we display in Fig. 7 the predicted contour lines for $\text{BR}(Z \rightarrow \tau\mu)$ as dashed lines. As expected from the correlation studied in Fig. 6, we see that these contour lines have approximately the same slope as the border of the exclusion region from $\text{BR}(\tau \rightarrow \mu\mu\mu)$, and in particular, the line corresponding to $\text{BR}(Z \rightarrow \tau\mu) = 2 \times 10^{-7}$ is very close to the upper bound line of the three body decay in all the TM scenarios (i.e., the border of the purple line). Furthermore, in the large M_R —large f region of these plots we see that for several TM scenarios, concretely TM-2, TM-3, TM-4, and TM-5, the $\text{BR}(\tau \rightarrow \mu\mu\mu)$ is the most constraining observable.

In contrast, in the low M_R and f region, the most constraining cLFV observable is the radiative decay

$\tau \rightarrow \mu\gamma$. On the other hand, regarding the flavor preserving observables, it is clear that the EWPO do not play a relevant role here, but both Δr_K and the invisible Z width put relevant constraints in some scenarios. In particular, Δr_K is the most constraining observable in the case of TM-8, and the Z invisible width is so in the scenarios TM-1, TM-6, and TM-7. We also learn that, typically, the Z invisible width is the most constraining observable in the region of low M_R values, whereas $\text{BR}(\tau \rightarrow \mu\mu\mu)$ is the most constraining observable in the region of high M_R values. Thus, generically, it is the crossing of these two excluded areas in the (M_R, f) plane that gives the focus area of the maximum allowed LFV Z decay rates, $\text{BR}(Z \rightarrow \tau\mu) \sim 2 \times 10^{-7}$, and this crossing occurs at different values of M_R and f in each scenario. For example, in the TM-4 and TM-5 scenarios it happens at $M_R \sim 2\text{--}4$ TeV and for $f \sim \mathcal{O}(1)$, while in the TM-6 M_R is around 10 TeV and $f \sim \mathcal{O}(2)$. On the other hand, if we focus our attention on the mass range of interest for present direct neutrino production searches at LHC, say masses around 1 TeV and below, we observe that the allowed $\text{BR}(Z \rightarrow \tau\mu)$ rates are smaller than this maximum value 2×10^{-7} ; nevertheless they are still in the reach of future linear colliders (10^{-9}) for some scenarios, such as TM-4 or TM-5.

Finally, we would like to end this section by comparing our results in Fig. 7 with previous results in the literature. In particular, we focus on Ref. [63], which to our knowledge is the only reference that provides predictions for the maximum allowed LFV Z decay rates in the same model, namely, the ISS with three RH neutrinos and three additional sterile states, which they refer to as the (3,3)-ISS realization. Their numerical results are scatter plots generated by random scans over the model parameter space, and for accommodating neutrino data they use the Casas-Ibarra parametrization, which provides the neutrino Yukawa couplings as output. The setup of the ISS model in their analysis is therefore different from ours, since we use the μ_X parametrization and Y_ν is an input. They provide the results in terms of their parameters $\tilde{\eta}$ and $\langle m_{4-9} \rangle$, whereas we present our results as contour lines in terms of f and M_R for the eight selected TM-*i* scenarios. The comparison can be done as follows: (1) Their $\langle m_{4-9} \rangle$ can be compared roughly with our M_R ; (2) Their parameter $\tilde{\eta}$ is defined as $\tilde{\eta} = 1 - |\text{Det}(\tilde{U}_{\text{PMNS}})|$ where $\tilde{U}_{\text{PMNS}} = (1 - \eta) U_{\text{PMNS}}$, and the matrix η is frequently used in the literature to encode the deviation of \tilde{U}_{PMNS} from unitarity (see, for instance, Refs. [68,69,71–73]). The \tilde{U}_{PMNS} can be compared with the complex conjugate of the 3×3 subblock of our unitary 9×9 matrix U^ν in Eq. (3) [or, similarly, with B_m in Eq. (9)]; (3) Our predicted maximum allowed BR's of the LFV Z decays are close to the contour line 10^{-7} and correspond to the region in the upper right corner of our plots for TM1-5 in Fig. 7. In order to compare with the results in Ref. [63] we have evaluated with our code the corresponding η and $\tilde{\eta}$ for the mentioned region, and we

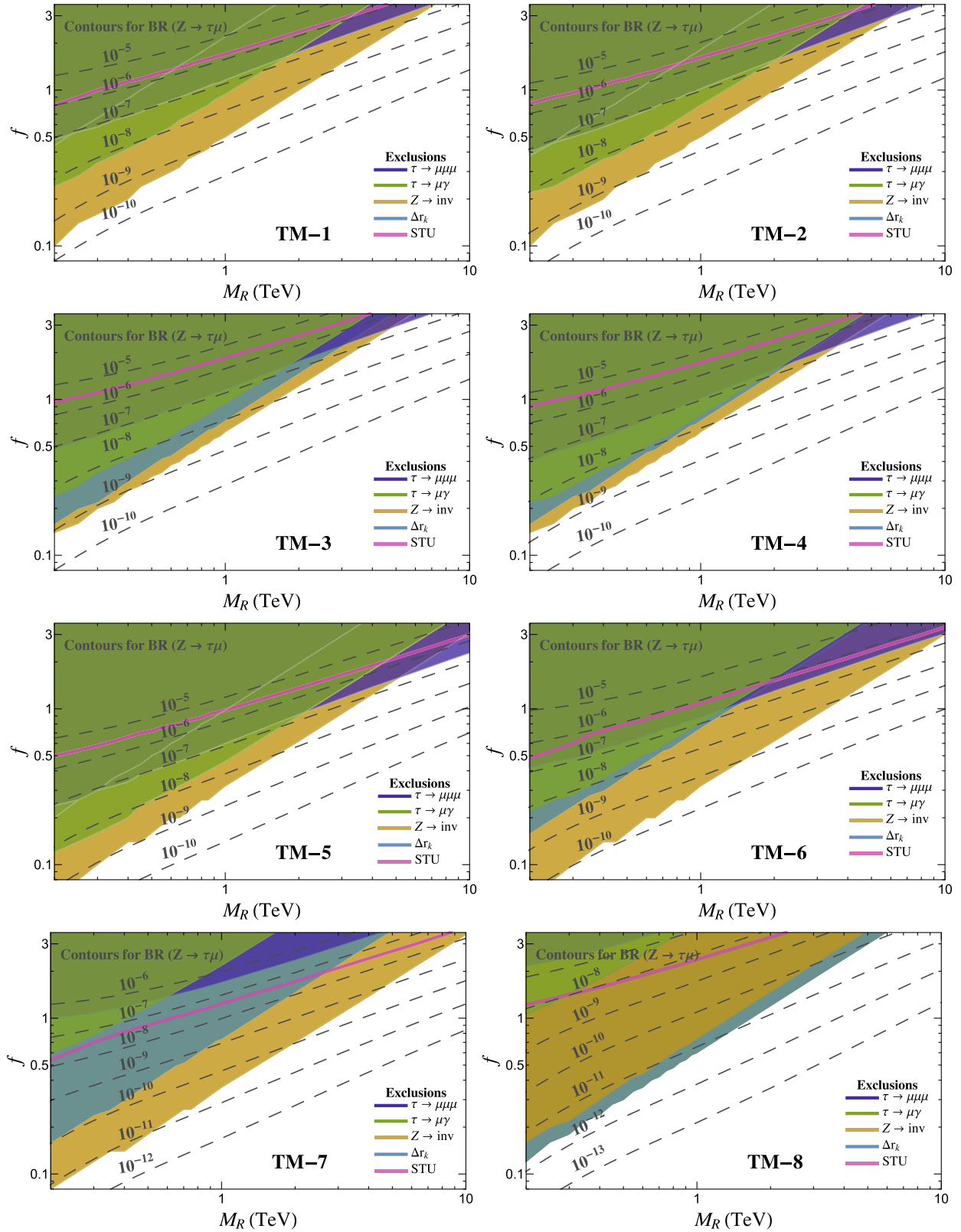


FIG. 7. Contour lines for $BR(Z \rightarrow \tau\mu)$ (dashed lines) in the (M_R, f) plane of the ISS model for the eight TM scenarios in Table III. Shaded areas are the excluded regions by $\tau \rightarrow \mu\mu\mu$ (purple), $\tau \rightarrow \mu\gamma$ (green), Z invisible width (yellow), and Δr_k (cyan). The region above the pink solid line is excluded by the S, T, U parameters. We obtain similar results for $BR(Z \rightarrow \tau e)$ in the TE scenarios by exchanging μ and e in these plots of the TM scenarios.

have compared them with the upper bounds found in the more recent literature about global constraints on heavy neutrino mixing. Concretely, we have used the recent results in Ref. [73], and we have applied them to the three sigma level in order to be in agreement with our choice for the rest of the constraints in this work.² This translates into an upper bound of $\tilde{\eta}^{\max} \simeq 6 \times 10^{-3}$. We have then checked that our predictions of LFV Z decays $\text{BR} \sim 10^{-7}$ in the upper right part of our plots (with $f = 1-3$ and $M_R = 6-10$ TeV) enter into the area allowed by this $\tilde{\eta}^{\max}$ constraint. More concretely, the crossing of the contour line for $\text{BR}(Z \rightarrow \tau\mu) \sim 10^{-7}$ with the contour line for $\tilde{\eta}^{\max} \simeq 6 \times 10^{-3}$ happens at $M_R \simeq 10, 8, 7, 6,$ and 7 TeV for TM-1, TM-2, TM-3, TM-4, and TM-5, respectively. In contrast, the results in Ref. [63] show that their maximum allowed LFV Z BR's are about 10^{-9} , and these are placed approximately at $\langle m_{4-9} \rangle \sim 10-100$ TeV and $\tilde{\eta} \sim 10^{-4}$. We also see that their predictions for the allowed LFV Z BR's are placed at $\tilde{\eta}$ below a maximum value which is in agreement with the above commented $\tilde{\eta}^{\max} \simeq 6 \times 10^{-3}$. Moreover, as previously noticed, we also agree with Ref. [63] in the correlation found between $\text{BR}(Z \rightarrow \tau\mu)$ and $\text{BR}(\tau \rightarrow \mu\mu\mu)$. However, our work contains predictions leading to $\text{BR}(\tau \rightarrow 3\mu)$ below but close to the present experimental limit, 2.1×10^{-8} , and allowed $\text{BR}(Z \rightarrow \tau\mu)$ close to 10^{-7} which are not contained in Ref. [63]. There are empty spaces in their plots, with no predictions, corresponding to points in the parameter space which are not reached by their scans. It is in some of those regions where we are finding the allowed LFV Z decay rates of order 10^{-7} by means of our selected directions in the (3,3)-ISS parameter space. Therefore we conclude that, although random scans with the Casas-Ibarra parametrization allow one to explore a large region of the parameter space and to study the general features of the model, they are not always optimal to reach specific directions along the parameter space. In particular, we infer that they seem to be inefficient in generating Yukawa textures leading to scenarios like ours, and as a consequence, they lead to lower allowed LFV Z decay rates. A similar conclusion was obtained in Ref. [58] in the context of the LFV Higgs decays, where the use of μ_X parametrization also provided larger allowed rates in these decays than with the Casas-Ibarra parametrization. Obviously, physics does not depend on the parametrization one chooses. However, the efficiency in reaching specific points/directions/areas in the parameter space does. In this sense, our study of the maximum allowed LFV Z decays is complementary to that in Ref. [63].

²We warmly acknowledge Josu Hernández-García for his valuable help in extracting the 3σ constraints from Ref. [73].

V. CONCLUSIONS

In this work we have studied several aspects of cLFV processes in the context of the ISS model. Motivated by the strong experimental upper bounds on LFV μ - e transitions, we have discussed a useful geometrical parametrization of the neutrino Yukawa coupling matrix that allows us to easily define ISS scenarios with suppressed LFV $_{\mu e}$. We have studied in full detail the LFV Z decays in these scenarios that are designed to find large rates for processes including a τ lepton, and we have investigated those that are allowed by all the present constraints. We have therefore fully explored in parallel also the most relevant constraints within this ISS-LFV $_{\mu e}$ model. Important constraints come from experimental upper bounds on the LFV three body lepton decays, since they are strongly correlated to the LFVZD in these scenarios. Taking into account all the relevant bounds, we found that heavy ISS neutrinos with masses in the few TeV range can induce maximal rates of $\text{BR}(Z \rightarrow \tau\mu) \sim 2 \times 10^{-7}$ and $\text{BR}(Z \rightarrow \tau e) \sim 2 \times 10^{-7}$ in the TM and TE scenarios, respectively, larger than what was found in previous studies. These rates are potentially measurable at future linear colliders and FCC-ee. Therefore, we have shown that searches for LFVZD at future colliders may be a powerful tool to probe cLFV in low scale seesaw models, in complementarity with low-energy (high-intensity) facilities searching for cLFV processes. Another appealing feature of our results is that the here presented improved sensitivity to LFVZD rates could come together with the possibility that the heavy neutrinos could be directly produced at LHC.

ACKNOWLEDGMENTS

We wish to thank warmly Ana M. Teixeira for the very interesting discussions on the subject studied in this work at the starting stages of this research. This work is supported by the European Union through the ITN ELUSIVES H2020-MSCA-ITN-2015//674896 and the RISE INVISIBLESPLUS H2020-MSCA-RISE-2015//690575, by the CICYT through Projects No. FPA2012-31880 and No. FPA2016-78645-P, by the Spanish Consolider-Ingenio 2010 Programme CPAN (CSD2007-00042), and by the Spanish MINECO's "Centro de Excelencia Severo Ochoa" Programme under Grant No. SEV-2012-0249. X. M. is supported through the FPU Grant No. AP-2012-6708. F. S. is supported through a grant from the Scuola di Scienze of the Università di Bologna.

APPENDIX A: LFV LEPTON DECAYS

For completeness, in this appendix we provide the needed formulas for the full one-loop computation of the LFV lepton decays in the particle mass basis, both the three body and the radiative decays, which we have implemented in our code.

The expression for the branching ratio $\text{BR}(\ell_m \rightarrow \ell_k \ell_k \ell_k)$ is taken from Refs. [6,74] as well as all the form factors required for its computation,

$$\begin{aligned} \text{BR}(\ell_m \rightarrow \ell_k \ell_k \ell_k) &= \frac{\alpha_W^4}{24576\pi^3} \frac{m_{\ell_m}^4}{m_W^4} \frac{m_{\ell_m}}{\Gamma_{\ell_m}} \times \left\{ 2 \left| \frac{1}{2} F_{\text{Box}}^{\ell_m \ell_k \ell_k \ell_k} + F_Z^{\ell_m \ell_k} - 2s_W^2 (F_Z^{\ell_m \ell_k} - F_\gamma^{\ell_m \ell_k}) \right|^2 \right. \\ &\quad + 16s_W^2 \text{Re} \left[\left(F_Z^{\ell_m \ell_k} + \frac{1}{2} F_{\text{Box}}^{\ell_m \ell_k \ell_k \ell_k} \right) G_\gamma^{\ell_m \ell_k} \right] - 48s_W^4 \text{Re} \left[(F_Z^{\ell_m \ell_k} - F_\gamma^{\ell_m \ell_k}) G_\gamma^{\ell_m \ell_k} \right] \\ &\quad \left. + 4s_W^4 |F_Z^{\ell_m \ell_k} - F_\gamma^{\ell_m \ell_k}|^2 + 32s_W^4 |G_\gamma^{\ell_m \ell_k}|^2 \left[\ln \frac{m_{\ell_m}^2}{m_{\ell_k}^2} - \frac{11}{4} \right] \right\}. \end{aligned} \quad (\text{A1})$$

The $\text{BR}(\ell_m \rightarrow \ell_k \ell_k \ell_k)$ contains several form factors, corresponding to the dipole, penguin (photon and Z), and box diagrams. The expressions for these form factors are given by [6,74]

$$\begin{aligned} G_\gamma^{\ell_m \ell_k} &= \sum_{i=1}^9 B_{\ell_k n_i} B_{\ell_m n_i}^* G_\gamma(x_i), \\ F_\gamma^{\ell_m \ell_k} &= \sum_{i=1}^9 B_{\ell_k n_i} B_{\ell_m n_i}^* F_\gamma(x_i), \\ F_Z^{\ell_m \ell_k} &= \sum_{i,j=1}^9 B_{\ell_k n_i} B_{\ell_m n_j}^* (\delta_{ij} F_Z(x_i) + C_{n_i n_j} G_Z(x_i, x_j) + C_{n_i n_j}^* H_Z(x_i, x_j)), \\ F_{\text{Box}}^{\ell_m \ell_k \ell_k \ell_k} &= \sum_{i,j=1}^9 B_{\ell_k n_i} B_{\ell_m n_j}^* (B_{\ell_k n_i} B_{\ell_k n_j}^* G_{\text{Box}}(x_i, x_j) + 2B_{\ell_k n_i}^* B_{\ell_k n_j} F_{\text{Box}}(x_i, x_j)), \end{aligned} \quad (\text{A2})$$

where x_i stands for the dimensionless ratio of masses ($x_i = m_{n_i}^2/m_W^2$). Moreover, the following loop functions enter in the previous form factors [6,74]:

$$\begin{aligned} F_Z(x) &= -\frac{5x}{2(1-x)} - \frac{5x^2}{2(1-x)^2} \ln x, \\ G_Z(x, y) &= -\frac{1}{2(x-y)} \left[\frac{x^2(1-y)}{1-x} \ln x - \frac{y^2(1-x)}{1-y} \ln y \right], \\ H_Z(x, y) &= \frac{\sqrt{xy}}{4(x-y)} \left[\frac{x^2-4x}{1-x} \ln x - \frac{y^2-4y}{1-y} \ln y \right], \\ F_\gamma(x) &= \frac{x(7x^2-x-12)}{12(1-x)^3} - \frac{x^2(x^2-10x+12)}{6(1-x)^4} \ln x, \\ G_\gamma(x) &= -\frac{x(2x^2+5x-1)}{4(1-x)^3} - \frac{3x^3}{2(1-x)^4} \ln x, \\ F_{\text{Box}}(x, y) &= \frac{1}{x-y} \left\{ \left(1 + \frac{xy}{4} \right) \left[\frac{1}{1-x} + \frac{x^2}{(1-x)^2} \ln x \right] - 2xy \left[\frac{1}{1-x} + \frac{x}{(1-x)^2} \ln x \right] - (x \rightarrow y) \right\}, \\ G_{\text{Box}}(x, y) &= -\frac{\sqrt{xy}}{x-y} \left\{ (4+xy) \left(\frac{1}{1-x} + x \frac{\ln x}{(1-x)^2} \right) - 2 \left(\frac{1}{1-x} + x^2 \frac{\ln x}{(1-x)^2} \right) - (x \rightarrow y) \right\}. \end{aligned} \quad (\text{A3})$$

In the limit of degenerate neutrino masses ($x = y$), we get the following expressions:

$$\begin{aligned}
G_Z(x, x) &= [x(-1 + x - 2 \ln x)/(2(1 - x))], \\
H_Z(x, x) &= -[x(4 - 5x + x^2 + (4 - 2x + x^2) \ln x)/(4(1 - x)^2)], \\
F_{\text{Box}}(x, x) &= [(4 - 19x^2 + 16x^3 - x^4 - 2x(-4 + 4x + 3x^2) \ln x)/(4(1 - x)^3)], \\
G_{\text{Box}}(x, x) &= x[(6 - 8x + 4x^2 - 2x^3 + (4 + x^2 + x^3) \ln x)/(-1 + x)^3].
\end{aligned} \tag{A4}$$

For the LFV radiative decay rates, we use the analytical formulas appearing in [6] and [96] that have also been implemented in our code,

$$\text{BR}(\ell_m \rightarrow \ell_k \gamma) = \frac{\alpha_W^3 s_W^2}{256 \pi^2} \left(\frac{m_{\ell_m}}{m_W} \right)^4 \frac{m_{\ell_m}}{\Gamma_{\ell_m}} |G_{mk}|^2, \tag{A5}$$

where Γ_{l_m} is total decay width of the lepton l_m , and

$$G_{mk} = \sum_{i=1}^9 B_{ki} B_{mi}^* G_\gamma(x_i), \tag{A6}$$

with $G_\gamma(x)$ defined in Eq. (A3) and, again, $x_i \equiv m_{n_i}^2/m_W^2$.

APPENDIX B: Δr_K

In this appendix we give the formulas to calculate the quantity Δr_K [see Eq. (22)], which parametrizes the deviation from the SM prediction arising from the sterile neutrinos contribution, as a test of lepton flavor universality. The expression for Δr_K in generic SM extension with sterile neutrinos has been given in [45]

$$\Delta r_K = \frac{m_\mu^2(m_K^2 - m_\mu^2)^2}{m_e^2(m_K^2 - m_e^2)^2} \frac{\sum_{i=1}^{N_{\text{max}}^{(e)}} |B_{en_i}|^2 [m_K^2(m_{n_i}^2 + m_e^2) - (m_{n_i}^2 - m_e^2)^2] \lambda^{1/2}(m_K, m_{n_i}, m_e)}{\sum_{j=1}^{N_{\text{max}}^{(\mu)}} |B_{\mu n_j}|^2 [m_K^2(m_{n_j}^2 + m_\mu^2) - (m_{n_j}^2 - m_\mu^2)^2] \lambda^{1/2}(m_K, m_{n_j}, m_\mu)} - 1, \tag{B1}$$

where $N_{\text{max}}^{e,\mu}$ is the heaviest neutrino mass eigenstate kinematically allowed in association with e or μ , respectively, and the kinematical function $\lambda(m_K, m_{n_i}, m_\ell)$ reads [45]

$$\lambda(a, b, c) = (a^2 - b^2 - c^2)^2 - 4b^2c^2. \tag{B2}$$

APPENDIX C: THE Z INVISIBLE DECAY WIDTH

The Z invisible decay width in the presence of massive Majorana neutrinos, as it is in the case of the present ISS model, reads [46]

$$\begin{aligned}
\Gamma(Z \rightarrow \text{inv})_{\text{ISS}} &= \sum_n \Gamma(Z \rightarrow nn)_{\text{ISS}} \\
&= \sum_{i \leq j=1}^{N_{\text{max}}} \left(1 - \frac{1}{2} \delta_{ij} \right) \frac{\sqrt{2} G_F}{48 \pi m_Z} \times \lambda^{1/2}(m_Z, m_{n_i}, m_{n_j}) \\
&\quad \times \left[2 |C_{n_i n_j}|^2 \left(2m_Z^2 - m_{n_i}^2 - m_{n_j}^2 - \frac{(m_{n_i}^2 - m_{n_j}^2)^2}{m_Z^2} \right) - 12 m_{n_i} m_{n_j} \text{Re}[(C_{n_i n_j})^2] \right],
\end{aligned} \tag{C1}$$

where N_{max} is the heaviest neutrino mass which is kinematically allowed and λ is given in Eq. (B2).

APPENDIX D: OBLIQUE PARAMETERS: S , T , U

The Majorana neutrino contributions to the S , T , U parameters have been computed in Ref. [89]. We apply those formulas to compute the sterile neutrinos contributions to the oblique parameters in the ISS model. The equation for the T parameter reads

$$T_{\text{tot}} = T_{\text{ISS}} + T_{\text{SM}} = \frac{-1}{8\pi s_W^2 m_W^2} \left\{ \sum_{\alpha=1}^3 m_{\ell_\alpha}^2 B_0(0, m_{\ell_\alpha}^2, m_{\ell_\alpha}^2) - 2 \sum_{i=1}^9 \sum_{\alpha=1}^3 |B_{\ell_\alpha n_i}|^2 Q(0, m_{n_i}^2, m_{\ell_\alpha}^2) \right. \\ \left. + \sum_{i,j=1}^9 (C_{n_i n_j} C_{n_j n_i} Q(0, m_{n_i}^2, m_{n_j}^2) + (C_{n_i n_j})^2 m_{n_i} m_{n_j} B_0(0, m_{n_i}^2, m_{n_j}^2)) \right\}, \quad (\text{D1})$$

where the index α refers to the charged leptons and

$$Q(q^2, m_1^2, m_2^2) \equiv (D-2)B_{00}(q^2, m_1^2, m_2^2) + q^2[B_1(q^2, m_1^2, m_2^2) + B_{11}(q^2, m_1^2, m_2^2)], \quad (\text{D2})$$

with $D \equiv 4 - 2\epsilon$ ($\epsilon \rightarrow 0$) and B_0, B_1, B_{11} , and B_{00} are the Passarino-Veltman functions [97] in the *LoopTools* [95] notation. The SM contribution can be cast as

$$T_{\text{SM}} = -\frac{1}{8\pi s_W^2 m_W^2} \left\{ 3Q(0, 0, 0) - 2 \sum_{\alpha=1}^3 Q(0, 0, m_{\ell_\alpha}^2) + \sum_{\alpha=1}^3 m_{\ell_\alpha}^2 B_0(0, m_{\ell_\alpha}^2, m_{\ell_\alpha}^2) \right\}, \quad (\text{D3})$$

where it has been used that the active neutrino masses are zero and the leptonic mixing matrix U is unitary in the SM. The equation for the S parameter is

$$S_{\text{tot}} = S_{\text{ISS}} + S_{\text{SM}} = -\frac{1}{2\pi m_Z^2} \left\{ \sum_{i,j=1}^9 C_{n_i n_j} C_{n_j n_i} \Delta Q(m_Z^2, m_{n_i}^2, m_{n_j}^2) + \sum_{i,j=1}^9 (C_{n_i n_j})^2 m_{n_i} m_{n_j} (B_0(0, m_{n_i}^2, m_{n_j}^2) - B_0(m_Z^2, m_{n_i}^2, m_{n_j}^2)) \right. \\ \left. + \sum_{\alpha=1}^3 m_{\ell_\alpha}^2 (B_0(0, m_{\ell_\alpha}^2, m_{\ell_\alpha}^2) - 2B_0(m_Z^2, m_{\ell_\alpha}^2, m_{\ell_\alpha}^2)) + Q(m_Z^2, m_{\ell_\alpha}^2, m_{\ell_\alpha}^2) \right\}, \quad (\text{D4})$$

where $\Delta Q(q^2, m_1^2, m_2^2) \equiv Q(0, m_1^2, m_2^2) - Q(q^2, m_1^2, m_2^2)$ and

$$S_{\text{SM}} = -\frac{1}{2\pi m_Z^2} \left\{ 3\Delta Q(m_Z^2, 0, 0) + \sum_{\alpha=1}^3 m_{\ell_\alpha}^2 (B_0(0, m_{\ell_\alpha}^2, m_{\ell_\alpha}^2) - 2B_0(m_Z^2, m_{\ell_\alpha}^2, m_{\ell_\alpha}^2)) + Q(m_Z^2, m_{\ell_\alpha}^2, m_{\ell_\alpha}^2) \right\}. \quad (\text{D5})$$

Finally, the U parameter is given by

$$U_{\text{tot}} = U_{\text{ISS}} + U_{\text{SM}} = \frac{1}{2\pi m_Z^2} \left\{ \sum_{i,j=1}^9 C_{n_i n_j} C_{n_j n_i} \Delta Q(m_Z^2, m_{n_i}^2, m_{n_j}^2) + \sum_{i,j=1}^9 (C_{n_i n_j})^2 m_{n_i} m_{n_j} (B_0(0, m_{n_i}^2, m_{n_j}^2) - B_0(m_Z^2, m_{n_i}^2, m_{n_j}^2)) \right. \\ \left. - \sum_{i=1}^9 \sum_{\alpha=1}^3 2 \frac{m_Z^2}{m_W^2} |B_{\ell_\alpha n_i}|^2 \Delta Q(m_W^2, m_{n_i}^2, m_{\ell_\alpha}^2) + \sum_{\alpha=1}^3 m_{\ell_\alpha}^2 (B_0(0, m_{\ell_\alpha}^2, m_{\ell_\alpha}^2) - 2B_0(m_Z^2, m_{\ell_\alpha}^2, m_{\ell_\alpha}^2)) - Q(m_Z^2, m_{\ell_\alpha}^2, m_{\ell_\alpha}^2) \right\}, \quad (\text{D6})$$

and its SM contribution reads

$$U_{\text{SM}} = \frac{1}{2\pi m_Z^2} \left\{ 3\Delta Q(m_Z^2, 0, 0) + \sum_{\alpha=1}^3 \left(m_{\ell_\alpha}^2 (B_0(0, m_{\ell_\alpha}^2, m_{\ell_\alpha}^2) - 2B_0(m_Z^2, m_{\ell_\alpha}^2, m_{\ell_\alpha}^2)) \right. \right. \\ \left. \left. - Q(m_Z^2, m_{\ell_\alpha}^2, m_{\ell_\alpha}^2) - 2 \frac{m_Z^2}{m_W^2} \Delta Q(m_W^2, 0, m_{\ell_\alpha}^2) \right) \right\}. \quad (\text{D7})$$

APPENDIX E: LFV Z DECAYS

For completeness, we give here the analytical expressions for LFV Z decay partial widths in the Feynman-t'Hooft gauge, which are obtained by computing the diagrams shown in Fig. 8. We take the results from [18,63] and adapt them to the

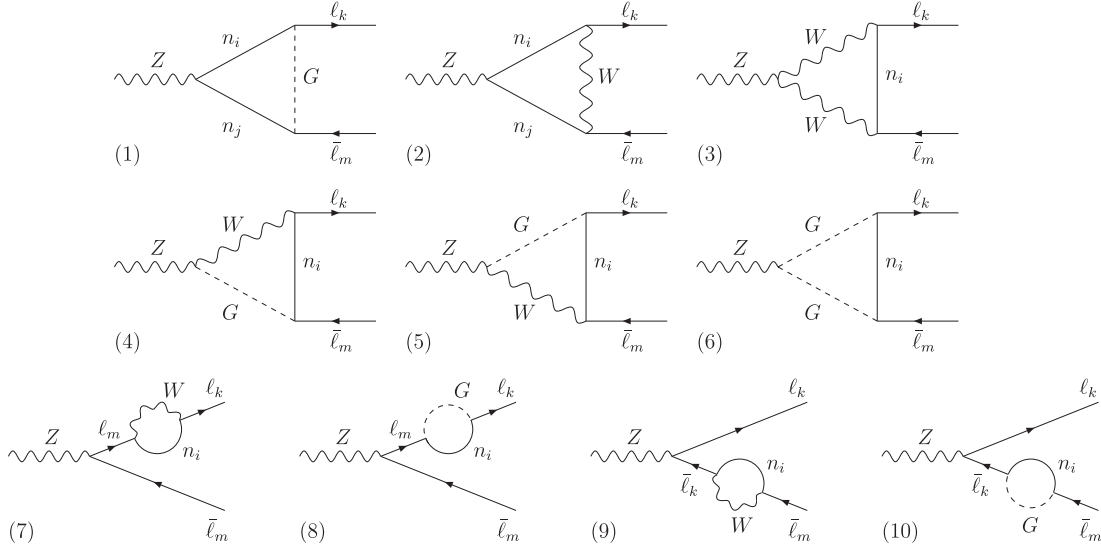


FIG. 8. One-loop diagrams in the Feynman-t'Hooft gauge for LFV Z decays with massive neutrinos.

notation introduced in Sec. II and to the convection of *LoopTools* [95] for the loop functions. Then, for $k \neq m$, we have

$$\Gamma(Z \rightarrow \ell_k \bar{\ell}_m) = \frac{\alpha_W^3}{192\pi^2 c_W^2} m_Z |\mathcal{F}_Z|^2, \quad (\text{E1})$$

with

$$\mathcal{F}_Z = \sum_{a=1}^{10} \mathcal{F}_Z^{(a)}. \quad (\text{E2})$$

The form factors of the different diagrams are

$$\begin{aligned} \mathcal{F}_Z^{(1)} = & \frac{1}{2} B_{\ell_k n_i} B_{\ell_m n_j}^* \left\{ -C_{n_i n_j} x_i x_j m_W^2 C_0 \right. \\ & \left. + C_{n_i n_j}^* \sqrt{x_i x_j} \left[m_Z^2 C_{12} - 2C_{00} + \frac{1}{2} \right] \right\}, \quad (\text{E3}) \end{aligned}$$

where $C_{0,12,00} \equiv C_{0,12,00}(0, m_Z^2, 0, m_W^2, m_{n_i}^2, m_{n_j}^2)$;

$$\begin{aligned} \mathcal{F}_Z^{(2)} = & B_{\ell_k n_i} B_{\ell_m n_j}^* \left\{ -C_{n_i n_j} [m_Z^2 (C_0 + C_1 + C_2 + C_{12}) \right. \\ & \left. - 2C_{00} + 1] + C_{n_i n_j}^* \sqrt{x_i x_j} m_W^2 C_0 \right\}, \quad (\text{E4}) \end{aligned}$$

where $C_{0,1,2,12,00} \equiv C_{0,1,2,12,00}(0, m_Z^2, 0, m_W^2, m_{n_i}^2, m_{n_j}^2)$;

$$\mathcal{F}_Z^{(3)} = 2c_W^2 B_{\ell_k n_i} B_{\ell_m n_j}^* \{ m_Z^2 (C_1 + C_2 + C_{12}) - 6C_{00} + 1 \}, \quad (\text{E5})$$

where $C_{1,2,12,00} \equiv C_{1,2,12,00}(0, m_Z^2, 0, m_{n_i}^2, m_W^2, m_W^2)$;

$$\mathcal{F}_Z^{(4)} + \mathcal{F}_Z^{(5)} = -2s_W^2 B_{\ell_k n_i} B_{\ell_m n_j}^* x_i m_W^2 C_0, \quad (\text{E6})$$

where $C_0 \equiv C_0(0, m_Z^2, 0, m_{n_i}^2, m_W^2, m_W^2)$;

$$\mathcal{F}_Z^{(6)} = -(1 - 2s_W^2) B_{\ell_k n_i} B_{\ell_m n_j}^* x_i C_{00}, \quad (\text{E7})$$

where $C_{00} \equiv C_{00}(0, m_Z^2, 0, m_{n_i}^2, m_W^2, m_W^2)$;

$$\begin{aligned} \mathcal{F}_Z^{(7)} + \mathcal{F}_Z^{(8)} + \mathcal{F}_Z^{(9)} + \mathcal{F}_Z^{(10)} \\ = \frac{1}{2} (1 - 2c_W^2) B_{\ell_k n_i} B_{\ell_m n_j}^* \{ (2 + x_i) B_1 + 1 \}, \quad (\text{E8}) \end{aligned}$$

where $B_1 \equiv B_1(0, m_{n_i}^2, m_W^2)$.

In all these formulas, sum over neutrino indices, $i, j = 1, \dots, 9$ has to be understood, $x_i \equiv m_{n_i}^2/m_W^2$, and the charged lepton masses have been neglected.

[1] P. Minkowski, *Phys. Lett.* **67B**, 421 (1977).

[2] M. Gell-Mann, P. Ramond, and R. Slansky, in *Supergravity*, edited by P. van Nieuwenhuizen and D. Z. Freedman (North-Holland, Amsterdam, 1979), p. 315.

[3] T. Yanagida, in *Proceedings of the Workshop on the Unified Theory and the Baryon Number in the Universe Report No. 79-18, Tsukuba, Japan*, edited by O. Sawada and A. Sugamoto (KEK, Tsukuba, 1979).

- [4] R. N. Mohapatra and G. Senjanovic, *Phys. Rev. Lett.* **44**, 912 (1980).
- [5] J. Schechter and J. W. F. Valle, *Phys. Rev. D* **22**, 2227 (1980).
- [6] A. Ilakovac and A. Pilaftsis, *Nucl. Phys.* **B437**, 491 (1995).
- [7] E. Arganda, A. M. Curiel, M. J. Herrero, and D. Temes, *Phys. Rev. D* **71**, 035011 (2005).
- [8] For a review on Majorana/Dirac neutrinos see, for instance E. Akhmedov, [arXiv:1412.3320](https://arxiv.org/abs/1412.3320).
- [9] G. Aad *et al.* (ATLAS Collaboration), *Phys. Rev. D* **90**, 072010 (2014).
- [10] G. Wilson, Neutrino Oscillations: are lepton-flavor violating Z decays observable with the CDR detector? and update on experimented aspects of lepton-flavor violating, in Proceedings of DESY-ECFA LC Workshop held at Frascati (1998).
- [11] G. Wilson, Neutrino Oscillations: are lepton-flavor violating Z decays observable with the CDR detector? and update on experimented aspects of lepton-flavour violating, in Proceedings of DESY-ECFA LC Workshop held at Oxford (1999).
- [12] A. Blondel, E. Graverini, N. Serra, and M. Shaposhnikov (FCC-ee Study Team Collaboration), *Nucl. Part. Phys. Proc.* **273–275**, 1883 (2016).
- [13] G. Mann and T. Riemann, *Ann. Phys. (Berlin)* **40**, 334 (1984).
- [14] J. Bernabeu, A. Santamaria, J. Vidal, A. Mendez, and J. W. F. Valle, *Phys. Lett. B* **187**, 303 (1987).
- [15] M. Dittmar, A. Santamaria, M. C. Gonzalez-Garcia, and J. W. F. Valle, *Nucl. Phys.* **B332**, 1 (1990).
- [16] J. G. Korner, A. Pilaftsis, and K. Schilcher, *Phys. Lett. B* **300**, 381 (1993).
- [17] A. Ilakovac, *Phys. Rev. D* **62**, 036010 (2000).
- [18] J. I. Illana, M. Jack, and T. Riemann, [arXiv:hep-ph/0001273](https://arxiv.org/abs/hep-ph/0001273).
- [19] J. I. Illana and T. Riemann, *Phys. Rev. D* **63**, 053004 (2001).
- [20] M. A. Perez, G. Tavares-Velasco, and J. J. Toscano, *Int. J. Mod. Phys. A* **19**, 159 (2004).
- [21] A. Flores-Tlalpa, J. M. Hernandez, G. Tavares-Velasco, and J. J. Toscano, *Phys. Rev. D* **65**, 073010 (2002).
- [22] D. Delepine and F. Vissani, *Phys. Lett. B* **522**, 95 (2001).
- [23] S. Davidson, S. Lacroix, and P. Verdier, *J. High Energy Phys.* **09** (2012) 092.
- [24] A. M. Baldini *et al.* (MEG Collaboration), *Eur. Phys. J. C* **76**, 434 (2016).
- [25] A. M. Baldini *et al.*, [arXiv:1301.7225](https://arxiv.org/abs/1301.7225).
- [26] B. Aubert *et al.* (BABAR Collaboration), *Phys. Rev. Lett.* **104**, 021802 (2010).
- [27] T. Aushev *et al.*, [arXiv:1002.5012](https://arxiv.org/abs/1002.5012).
- [28] U. Bellgardt *et al.* (SINDRUM Collaboration), *Nucl. Phys.* **B299**, 1 (1988).
- [29] A. Blondel *et al.*, [arXiv:1301.6113](https://arxiv.org/abs/1301.6113).
- [30] K. Hayasaka *et al.*, *Phys. Lett. B* **687**, 139 (2010).
- [31] K. Hayasaka, [arXiv:1010.3746](https://arxiv.org/abs/1010.3746).
- [32] W. H. Bertl *et al.* (SINDRUM II Collaboration), *Eur. Phys. J. C* **47**, 337 (2006).
- [33] C. Dohmen *et al.* (SINDRUM II Collaboration), *Phys. Lett. B* **317**, 631 (1993).
- [34] A. Alekou *et al.*, [arXiv:1310.0804](https://arxiv.org/abs/1310.0804).
- [35] Y. Kuno (COMET Collaboration), *Prog. Theor. Exp. Phys.* **2013**, 022C01 (2013).
- [36] R. M. Carey *et al.* (Mu2e Collaboration), Report No. FERMILAB-PROPOSAL-0973, 2008.
- [37] R. Akers *et al.* (OPAL Collaboration), *Z. Phys. C* **67**, 555 (1995).
- [38] P. Abreu *et al.* (DELPHI Collaboration), *Z. Phys. C* **73**, 243 (1997).
- [39] G. Aad *et al.* (ATLAS Collaboration), *Eur. Phys. J. C* **77**, 70 (2017).
- [40] CMS Collaboration, Report No. CMS-PAS-HIG-14-040, 2015.
- [41] V. Khachatryan *et al.* (CMS Collaboration), *Phys. Lett. B* **749**, 337 (2015).
- [42] R. N. Mohapatra, *Phys. Rev. Lett.* **56**, 561 (1986).
- [43] R. N. Mohapatra and J. W. F. Valle, *Phys. Rev. D* **34**, 1642 (1986).
- [44] M. C. Gonzalez-Garcia and J. W. F. Valle, *Mod. Phys. Lett. A* **07**, 477 (1992).
- [45] A. Abada, D. Das, A. M. Teixeira, A. Vicente, and C. Weiland, *J. High Energy Phys.* **02** (2013) 048.
- [46] A. Abada, A. M. Teixeira, A. Vicente, and C. Weiland, *J. High Energy Phys.* **02** (2014) 091.
- [47] A. Abada and T. Toma, *J. High Energy Phys.* **02** (2016) 174.
- [48] A. Abada and T. Toma, *J. High Energy Phys.* **08** (2016) 079.
- [49] A. Abada, V. De Romeri, and A. M. Teixeira, *J. High Energy Phys.* **09** (2014) 074.
- [50] C.-Y. Chen and P. S. B. Dev, *Phys. Rev. D* **85**, 093018 (2012).
- [51] P. S. Bhupal Dev, R. Franceschini, and R. N. Mohapatra, *Phys. Rev. D* **86**, 093010 (2012).
- [52] A. Das and N. Okada, *Phys. Rev. D* **88**, 113001 (2013).
- [53] A. Das, P. S. Bhupal Dev, and N. Okada, *Phys. Lett. B* **735**, 364 (2014).
- [54] E. Arganda, M. J. Herrero, X. Marcano, and C. Weiland, *Phys. Lett. B* **752**, 46 (2016).
- [55] A. Das and N. Okada, *Phys. Rev. D* **93**, 033003 (2016).
- [56] A. Das, P. Konar, and S. Majhi, *J. High Energy Phys.* **06** (2016) 019.
- [57] A. Abada, G. Arcadi, and M. Lucente, *J. Cosmol. Astropart. Phys.* **10** (2014) 001.
- [58] E. Arganda, M. J. Herrero, X. Marcano, and C. Weiland, *Phys. Rev. D* **91**, 015001 (2015).
- [59] E. Arganda, M. J. Herrero, X. Marcano, and C. Weiland, *Phys. Rev. D* **93**, 055010 (2016).
- [60] A. Abada, D. Das, A. Vicente, and C. Weiland, *J. High Energy Phys.* **09** (2012) 015.
- [61] A. Abada, M. E. Krauss, W. Porod, F. Staub, A. Vicente, and C. Weiland, *J. High Energy Phys.* **11** (2014) 048.
- [62] A. Abada, V. De Romeri, and A. M. Teixeira, *J. High Energy Phys.* **02** (2016) 083.
- [63] A. Abada, V. De Romeri, S. Monteil, J. Orloff, and A. M. Teixeira, *J. High Energy Phys.* **04** (2015) 051.
- [64] A. Abada, D. Bečirević, M. Lucente, and O. Sumensari, *Phys. Rev. D* **91**, 113013 (2015).
- [65] B. Pontecorvo, *Zh. Eksp. Teor. Fiz.* **33**, 549 (1957) [*Sov. Phys. JETP* **6**, 429 (1957)].
- [66] Z. Maki, M. Nakagawa, and S. Sakata, *Prog. Theor. Phys.* **28**, 870 (1962).

- [67] M. C. Gonzalez-Garcia, M. Maltoni, and T. Schwetz, *J. High Energy Phys.* **11** (2014) 052.
- [68] S. Antusch, C. Biggio, E. Fernandez-Martinez, M. B. Gavela, and J. Lopez-Pavon, *J. High Energy Phys.* **10** (2006) 084.
- [69] E. Fernandez-Martinez, M. B. Gavela, J. Lopez-Pavon, and O. Yasuda, *Phys. Lett. B* **649**, 427 (2007).
- [70] F. del Aguila, J. de Blas, and M. Perez-Victoria, *Phys. Rev. D* **78**, 013010 (2008).
- [71] S. Antusch, J. P. Baumann, and E. Fernandez-Martinez, *Nucl. Phys.* **B810**, 369 (2009).
- [72] S. Antusch and O. Fischer, *J. High Energy Phys.* **10** (2014) 094.
- [73] E. Fernandez-Martinez, J. Hernandez-Garcia, and J. Lopez-Pavon, *J. High Energy Phys.* **08** (2016) 033.
- [74] R. Alonso, M. Dhen, M. B. Gavela, and T. Hambye, *J. High Energy Phys.* **01** (2013) 118.
- [75] V. Cirigliano and I. Rosell, *Phys. Rev. Lett.* **99**, 231801 (2007).
- [76] M. Finkemeier, *Phys. Lett. B* **387**, 391 (1996).
- [77] E. Goudzovski (NA48/2, NA62 Collaborations), *Proc. Sci., EPS-HEP2011* (2011) 181 [arXiv:1111.2818].
- [78] C. Lazzeroni *et al.* (NA62 Collaboration), *Phys. Lett. B* **719**, 326 (2013).
- [79] K. A. Olive *et al.* (Particle Data Group Collaboration), *Chin. Phys. C* **38**, 090001 (2014).
- [80] E. Fernandez-Martinez, J. Hernandez-Garcia, J. Lopez-Pavon, and M. Lucente, *J. High Energy Phys.* **10** (2015) 130.
- [81] P. Benes, A. Faessler, F. Simkovic, and S. Kovalenko, *Phys. Rev. D* **71**, 077901 (2005).
- [82] M. Blennow, E. Fernandez-Martinez, J. Lopez-Pavon, and J. Menendez, *J. High Energy Phys.* **07** (2010) 096.
- [83] A. Abada and M. Lucente, *Nucl. Phys.* **B885**, 651 (2014).
- [84] M. Agostini *et al.* (GERDA Collaboration), *Phys. Rev. Lett.* **111**, 122503 (2013).
- [85] M. Auger *et al.* (EXO-200 Collaboration), *Phys. Rev. Lett.* **109**, 032505 (2012).
- [86] J. B. Albert *et al.* (EXO-200 Collaboration), *Nature (London)* **510**, 229 (2014).
- [87] A. Gando *et al.* (KamLAND-Zen Collaboration), *Phys. Rev. Lett.* **110**, 062502 (2013).
- [88] M. E. Peskin and T. Takeuchi, *Phys. Rev. D* **46**, 381 (1992).
- [89] E. Akhmedov, A. Kartavtsev, M. Lindner, L. Michaels, and J. Smirnov, *J. High Energy Phys.* **05** (2013) 081.
- [90] A. Atre, T. Han, S. Pascoli, and B. Zhang, *J. High Energy Phys.* **05** (2009) 030.
- [91] D. V. Forero, M. Tortola, and J. W. F. Valle, *Phys. Rev. D* **86**, 073012 (2012).
- [92] G. L. Fogli, E. Lisi, A. Marrone, D. Montanino, A. Palazzo, and A. M. Rotunno, *Phys. Rev. D* **86**, 013012 (2012).
- [93] D. V. Forero, M. Tortola, and J. W. F. Valle, *Phys. Rev. D* **90**, 093006 (2014).
- [94] R. Adhikari *et al.*, *J. Cosmol. Astropart. Phys.* **01** (2017) 025.
- [95] T. Hahn and M. Perez-Victoria, *Comput. Phys. Commun.* **118**, 153 (1999).
- [96] F. Deppisch and J. W. F. Valle, *Phys. Rev. D* **72**, 036001 (2005).
- [97] G. Passarino and M. J. G. Veltman, *Nucl. Phys.* **B160**, 151 (1979).